UNIVERSIDADE FEDERAL DO RIO GRANDE DO SUL
INSTITUTO DE INFORMÁTICA
PROGRAMA DE PÓS-GRADUAÇÃO EM COMPUTAÇÃO

ANDRE LUÍS BELING DA ROSA

An Accessible Approach for Corneal Topography

Thesis presented in partial fulfillment
of the requirements for the degree of
Master of Computer Science

Prof. Dr. Manuel Menezes de Oliveira Neto
Advisor

Porto Alegre, december 2013

CIP – CATALOGING-IN-PUBLICATION

Rosa, Andre Luís Beling da

An Accessible Approach for Corneal Topography / Andre Luís Beling da Rosa. – Porto Alegre: PPGC da UFRGS, 2013.

79 f.: il.

Thesis (Master) – Universidade Federal do Rio Grande do Sul. Programa de Pós-Graduação em Computação, Porto Alegre, BR–RS, 2013. Advisor: Manuel Menezes de Oliveira Neto.

1. Corneal topography. 2. Image processing. 3. Zernike polynomials. 4. Geometric reconstruction. I. Oliveira Neto, Manuel Menezes de. II. Title.

“Whether you think you can, or you think you can’t — you are right.”
— HENRY FORD

ACKNOWLEDGMENTS

First, I would like to thank to my family for the support they have given to me in all my life, this support have been very important in my way to here. I really thank my girlfriend by her patience during the writing of this thesis, it take much time that would be together.

I thank to Manuel, my advisor, for his guidance during the masters and the thesis writing. I also thank to my colleagues and professors from CG group, they had supplied many important resources to me to finish this work.

Thank very much all.

ABSTRACT

Corneal topography consists of measuring the corneal shape, which is a key factor for visual acuity. The exam is used, for instance, in keratoconus detection, personalized contact lens fitting, in pre- and post-procedures associated with refractive surgery and corneal transplants. This thesis presents an accessible, inexpensive and portable approach to perform corneal topographies. The results obtained with our prototype show a mean difference of about 0.02 millimeters, equivalent to 0.5% of the mean corneal radius, when compared to topographies acquired with a commercial device. Our approach is based on Placido's disks, a set of concentric disks that are placed in front of the patient's eye and reflected on the cornea. Observing the deformation of the projected pattern, one can identify some refractive conditions (e.g., astigmatism, keratoconus) and estimate the patient's corneal topography. We have built a clip-on device to be used with a cell phone to emit the patterns, which are then captured by the cell phone camera. We use a software pipeline to enhance the images, segment the patterns, associate the emitted pattern with the captured one to sample the signal, and finally estimate the corneal surface. The estimated shape is then decomposed using Zernike polynomials in components with specific optical meanings. We have evaluated the results obtained with our prototype in three ways: visual inspection of keratoscopies, keratoconus detection, and comparison with the results produced by a commercial corneal topographer. According to such analysis, our device can be used for screening of individuals with keratoconus, and to obtain corneal topographies with 0.02-millimeter differences with respect to the results obtained with a commercial corneal topographer.

Keywords: Corneal topography, Image processing, Zernike polynomials, Geometric reconstruction.

Uma abordagem acessível para topografia da córnea

RESUMO

Topografias da córnea consistem em medir a forma da córnea, que é um fator chave para a acuidade visual. O exame é usado, por exemplo, na detecção de ceratocone, ajuste personalizado de lentes de contato, e pre e pós procedimentos associados com cirurgias refrativas e transplante de córnea. Esta dissertação apresenta, uma abordagem acessível e portátil para realizar topografias da córnea. Os resultados obtidos com o nosso protótipo mostram uma diferença média por volta de 0.02 milimetros, equivalente a 0.5% do raio médio da córnea, quando comparadas com topografias adquiridas com um topografo comercial. Nossa abordagem é baseada no disco de Plácido, a um conjunto de círculos concêntricos que são colocados na frente do olho do paciente e refletidos na córnea. Observando a deformação do padrão projetado, podemos identificar algumas condições refrativas (e.g. astigmatismo, ceratocone) e estimar a topografia da córnea do paciente. Nós construimos um dispositivo para ser utilizado com um celular para emitir os padrões, estes são então capturados pela câmera do celular. Nós usamos um sequência de procedimentos para melhor as imagens, segmentar os padrões, associar o padrão capturado com o emitido para amostrar o sinal, e finalmente estimar a superfície da córnea. A forma estimada é então decomposta, usando-se os polinômios de Zernike, em componentes com significado ótico específico. Nós avaliamos os resultados obtidos com o nosso protótipo de três maneiras: inspeção visual de ceratoscopias, detecção de ceratocone, e comparação com os resultados produzidos por um topográfo de córnea comercial. De acordo com essa análise, nosso dispositivo pode ser utilizado para o exame de indivíduos com ceratocone, e obter topografias com 0.02 milimetros de diferença em relação aos resultados obtidos com um topógrafo comercial.

Palavras-chave: Topografia da córnea, Processamento de imagens, Polinômios de Zernike, Reconstrução de geometria.

LIST OF FIGURES

LIST OF TABLES

TABLE OF CONTENTS

1 INTRODUCTION

Technology evolution makes many electronic devices very accessible. However, this is not a reality in all applications. Corneal topography is a field that still has high costs. In ophthalmology, it has applications in keratoconus diagnosis, refractive surgery pre and post procedures, and contact lens fitting. The first method to examine corneal topography is the Placido's disk (PLACIDO, 1880). It is basically a disk with concentric alternating black and white circles, with a hole in the center. The observer looks into the subject's eye through the hole and sees the circles deformations defined by the cornea's surface. This method evolved to automatic approaches where the assayer eye is replaced by a camera (see Figure 1.1) and image processing techniques are used to reconstruct an accurate corneal map.

There are three main types for corneal reconstruction methods, which are based on: specular reflections using Placido's disk; triangulation from structured light; and interferometry (KLEIN, 2000). Approaches inspired by Placidos's disk use concentric ring patterns that are reflected into corneal surface and captured by a sensor. Corneal topography is reconstructed from the pattern deformations captured at the sensor. Triangulation methods use structured-light sources (a chess pattern for example), diffusely reflected on the cornea and also captured by a camera. Since corneas produce specular reflections, some approach needs to be used to produce diffuse reflections. These might include the use ultraviolet light in the source; and use sodium fluorescein in the eye which is illuminated with blue light (SCHWIEGERLING, 2004). A basic difference between these two methods are the way measures are made: specular-reflection-based techniques measure slopes; triangulation approaches calculate heights. Finally, interferometry-based approaches use a light source interference pattern from reflections into the cornea and a reference shape to measure corneal shape. Methods based on interferometry are the most accurate ones, but they are very sensitive. Due to support techniques needed for triangulation and high complexity for interferometry, a low-cost device is easily achieved using an approach inspired in the Placido's disk.

To build a topographer it is necessary: a pattern (i.e. concentric circles) source; a device to capture the surface with the reflected pattern; and a device to process the reconstruction algorithm. These are relatively simple requirements to meet, but an accessible topographer was not built yet. We aim to confirm the intuition and build this topographer. We also aim to discover the topographer's accuracy in comparison with commercial equipments and their possible applications.

Figure 1.1: Placido's disk based on corneal condition diagnosis.

The Placido's topographer was first conceived for manual use (a), where an observer looks into the reflected pattern through a hole in the disk. Modern topographers based on Placido's disk replaced the observer by a camera (b). The captured images are processed in order to estimate the corneal surfaces.

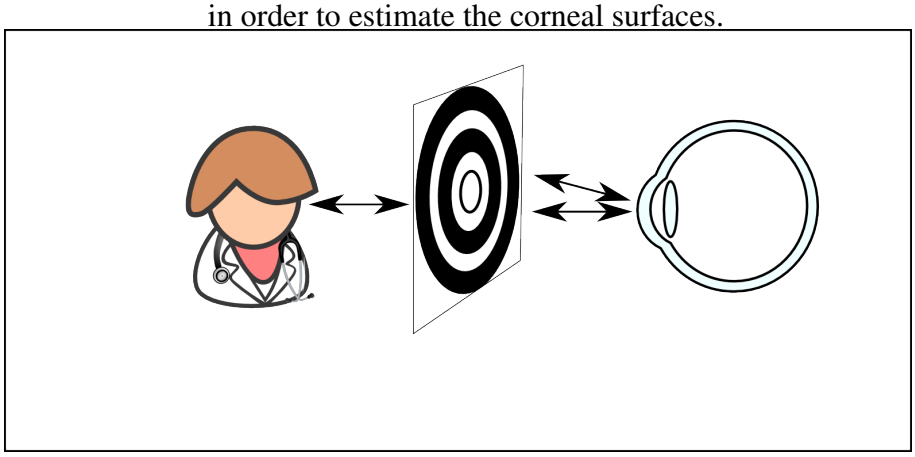

(a) Manual assessments with placido's disk

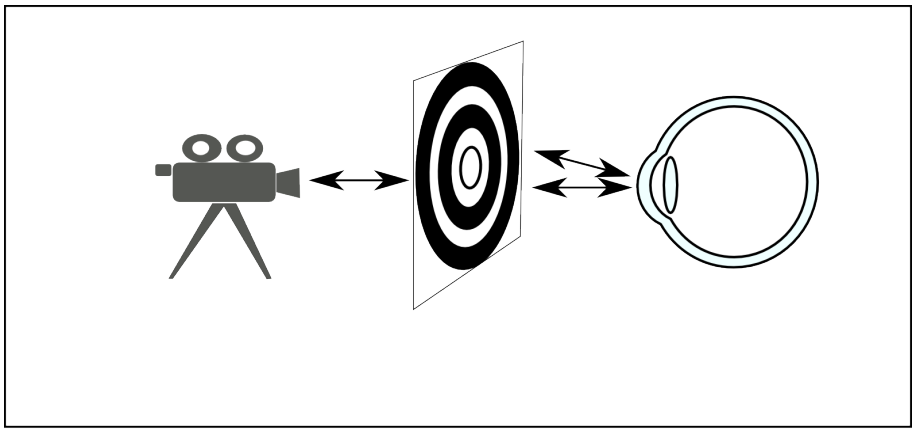

(b) Modern systems based on placido's disk

1.1 Thesis Statement

It is possible to build an inexpensive and portable corneal topographer based on Placido's disk. Using this topographer it is possible to assist in corneal-condition diagnoses.

To demonstrate this thesis, we need to overcome some challenges. First, we need to create an inexpensive and portable device to capture an image with the Placido's disks. This image needs to be good enough to extract the patterns. Second, the pattern needs to be correctly segmented from the captured image. Due to the restriction to build the device, cost and portability, these algorithms need to compensate poor quality in the captured image. Third, we need to correctly associate the extracted patterns with the source ones. This is very important to the reconstruction phase.

We demonstrate our thesis by building a prototype that can capture an image with the Placido's disk and implementing the next steps of the pipeline until the corneal surface estimation. In details, we enhance a cell-phone with a clip-on device containing a pattern to capture the desired image; we design an algorithm pipeline to extract the rings reflected on the cornea; we developed an algorithm to associate the rings in the captured image and in the pattern emitter; and finally, we apply reconstruction and modeling algorithm

from literature (KLEIN, 1992; SCHWIEGERLING; GREIVENKAMP, 1997) to obtain the corresponding corneal topography.

1.2 Structure of this Thesis

The remaining of this thesis is organized as follow: Chapter 2 reviews the available commercial topographers and discusses corneal-topography related techniques in the literature. Chapter 3 presents the fundamentals to understand the rest of the thesis. It introduces fundamental concepts about the human eye, corneal topography, and corneal modeling. In Chapter 4, we describe our prototype development and the algorithms used to estimate the corneal surface. In Chapter 5, we discuss the results we get using our proposal. And finally, Chapter 6 concludes the thesis and discusses possible future works.

2 RELATED WORK

Several topographers are available in the market to assist the medical needs. In this chapter we present different topographers and their features. Further, we cite works that created accessible ophthalmological devices. Finally, we discuss works that process the data captured by the topographers.

2.1 Comercial Topographers

Many topographers are commercially available, including handheld devices. We present these devices and some technical details.

The company EyeSys Vision has two topographers, both based on the Placido's disk approach; the System 3000 (EYESYS, 2010a) and the Vista (EYESYS, 2010b). The first is a desk topographer that calculates corneal topography and pupillometry (Figure 2.2(a)). The Vista is a portable device, and their creators claim that it can be used to exam in all clinical environments, including surgery rooms. It can be also used mounted on a slip-lamp to be used as a desk topographer. The image acquisition is automatic, containing 26 Placido's rings and capturing 9360 points on the corneal surface. Figure 2.1 shows the EyeSys topographers.

Figure 2.1: EyeSys Vision corneal topographers.

(a) System 3000 (b) Vista

Images from (EYESYS, 2010a,b)

Carleton Optical has also two topographer models, one for desk and one for handheld use; the Bon Optic Eye Top (CARLETON, n.d.a) and the Bon Optic Eye top 2H (CARLETON, n.d.b), shown in Figure 2.2. The Bon Optic Eye Top also performs corneal topography and pupillomery, and is based on Placido's disk using 24 rings. The measurement zone up to 10 mm, and has repeatability with a 0.01 diopter accuracy. The other model is the portable one. It is similar to the company's other model: 24 rings and 10 mm measurement zone, and also the same repeatability value. Moreover, it can be

used attached into some slit-lamp devices.

Figure 2.2: Bon Optics corneal topographers.

(a) Bon Optic Eye Top (b) Bon Optic Eye Top 2H

Images from (CARLETON, n.d.a,n)

The CSO Opthalmic has 3 topographers: the CM02 (CSO, n.d.a), a desk topographer; the Eye Top Lite (CSO, n.d.b), a version with less resources; and finally, the Focus (CSO, n.d.c), a portable model; all based on the Placido's disk approach. The CM02 has 24 rings and a 92 mm work distance, capturing images at 25 frames per second and 768x576 pixels. The topographer tries to get the best focus image, and consequently, a better exam result. In addition, the topographer's software performs an automatic rigid lens search based on the topography information. The Lite version has a more accessible price and less features. It also has 24 rings, but its work distance is 58 mm. It also uses best focus and the contact lens search. Finally, the Focus is the portable topographer. Like the other portable topographers, it was developed to be used in all clinical environments, including surgery rooms, and can be attached to a slit-lamp device. Its features are similar to the other company topographers: 24 rings, 56 mm work distance, and 25 frames per second (768x576 px). It also has the best-focus and lens-selection algorithms. The three models are shown in Figure 2.3.

Figure 2.3: CSO corneal topographers.

(a) CM02 (b) Eye Top Lite (c) Focus

Images from (CSO, n.d.b,n,n)

Opticon has 4 topographer models (see Figure 2.4): Keratron (OPTIKON, n.d.a) is the desk topographer; the Keratron Scout (OPTIKON, n.d.b) is the portable topographer, when using a battery, or can also be used together with a slit-lamp; the Keratron Piccolo (OPTIKON, n.d.c) was developed to be a more accessible version; finally, the Keratron Onda (OPTIKON, n.d.d) uses the same technology as the other Opticon topographers

and also has an ocular aberrometer. The 4 topographers are based on Placido's disk, have 28 rings and cover 90% of the corneal surface. Additionally, they also capture images at best focus.

Figure 2.4: Opticon corneal topographers.

(a) Keratron (b) Keratron Scout

(c) Keratron Piccolo (d) Keratron Onda

Images from (OPTIKON, n.d.a,n,n,n)

The company Medmont has a topographer called E300 (MEDMONT, 2012), — Figure 2.5. The E300 is a desk topographer based on Placido's disk. It uses 32 rings and performs 9,600 measurements during the exam. It covers the cornea from 0.25 mm to 10 mm radius. Its software selects a best focus image to perform the image capture and also has an automatic lens selection.

The Oculus Pentacam (OCULUS, 2012) is a device that uses slit ilummination and a Scheimpflug camera to get several eye measurements. The Scheimplug principle provides the focal plane orientation, when the lens and sensor planes are not parellel (MERKLINGER, 1996). Using this principle, the camera can capture a sharp eye image from cornea to crystalline. Several images are captured, the camera rotates to get images of various meridians. After that, the captured images are processed and assembled to build a three-dimensional reconstruction of the eye's anterior chamber (cornea, crystalline, etc). From this, it is possible to calculate information about the eye such as, for example, anterior and posterior corneal elevation, and cornea thickness. Figure 2.6 shows the topographer.

The company Ziemer Ophthalmology combines two tecnologies in its topographer, called Galilei (ZIEMER, n.d.), Figure 2.7. It uses the Placido's disk approach and the Scheimpflug principle to capture an image. The results from the two techniques are combined to produce a result with the advantages from the two techniques, accurate curvature, from Placido's disk, and accurate height, from Scheimpflug.

Figure 2.5: Medmont corneal topographer.

Figure from (MEDMONT, 2012)

Figure 2.6: Oculus corneal topographer.

Image from (OCULUS, 2012)

Another topographer that combines the Placido's disk and the Scheimpflug principle is the TMS-5 from Tomey (TOMEY, 2011). Its measurement time is around 1 second. It uses 25 to 31 rings capturing 256 point per ring. Figure 2.8 shows the TMS-5.

The CSO Italia offers two topographers: MODI'02 and SIRIUS (ITALIA, n.d.) (see figure 2.10). The MODI'02 is a topographer designed for users starting with corneal topography. While the model SIRIUS offers much more detailed information, it also uses the Placido's and Scheimpflug's combination to improve the results.

The Orbscan performs corneal height measurements using triangulation methods. While approaches based on Placido's disk use specular reflection, the Orbscan uses diffuse reflection. A slit lamp and a camera are used to triangulate a corneal height at a corneal point. This equipment has a low measurement repeatability due to the used approach. To solve this, the Orbscan II also employs a keratometer, that uses specular reflections. This way, the new Orbscan version combines these two informations to improve their results (AGARWAL; AGARWAL; JACOB, 2009).

The AstraMax from LaserSight (SIGHT, n.d.), see Figure 2.9, is a topographer that uses 3 cameras to triangulate the position from a narrow slit beam. Its cameras capture the light passing through the cornea in several moments, allowing it to take different corneal measurements, as for instance, the corneal thickness. The equipment captures 35,000 points in less than 0.2 seconds.

Figure 2.7: Ziemer corneal topographer.

Image from (ZIEMER, n.d.)

Figure 2.8: Tomey corneal topographer.

Image from (TOMEY, 2011)

2.2 Accessible Devices

Pamplona et al. (PAMPLONA et al., 2010) proposed a device based on a smartphone for estimating refractive errors, such as myopia, hyperopia and astigmatism. They use an iterative process where the subject looks through a clip-on attached to the smartphone and tries to align two line segments.

The idea is to use the Shack-Hartmann fundamentals in an inverse way. The Shack-Hartmann device has a laser that is target at the retina and the light reflex, refracted by eye lenses, is captured by a sensor. The place where the points are captured depends on the optical power in the eye, hence a greater or smaller optical power will change the result in the sensor. NETRA does the inverse process, it puts two lines in different positions and asks the subject to align them. When this happens, the distance between the two lines in the sensor is related to the subject condition. Figure 2.11 illustrates NETRA being used.

In a posterior work, Pamplona et al. (PAMPLONA et al., 2011) introduced a smartphone-based device, to detect and measure cataracts. Like NETRA, CATRA uses a clip-on attached to the smartphone to perform the assessment. The idea is to control the light rays' directions that reach the crystalline, where the cataract evolves. When the rays reach a region with cataracts, the light is diffused and the subject sees a blur. To control the light direction, a pinhole is placed in front of the smartphone's display, and only specific pixels are turned on. To get the assessment, basically, the device scans the eye, using light rays in different directions, and the user provides some feedback when he sees a blurred spot. Hence, the system detects the presence of cataracts and produces a location map.

Figure 2.9: LaserSight corneal topographer.

Image from (SIGHT, n.d.)

Figure 2.10: CSO Italia corneal topographers.

(a) MODI 02 (b) Sirius

Images from (ITALIA, n.d.)

2.3 Reconstruction Techniques

Doss et al. (DOSS et al., 1981) introduced a method to reconstruct the corneal surface from captured Placido's disk images, called *Arc-step* algorithm. The basic idea of the algorithm is, for each point pair next to the other in a corneal meridian (Figure 2.12(a)), find an arc that connects these two points — Figure 2.12(b). To find such arcs, a few restrictions are used, see Figure 2.12(c). The first point needs to preserve its normal and local curvature. Also the next point's normal needs to respect the law of reflection, considering the incoming and reflected light rays calculated from the captured image and pattern position. The process is iterative, and, at each step, the solution is improved until a solution is found, based on a threshold. After, the next point is calculated until the last ring. Figure 2.12(d) depicts this.

An approach based on B-splines was proposed by Halstead et. al. (HALSTEAD et al., 1996). Their algorithm starts with a guess for an initial surface. A ray-tracing is performed using this surface and compared with the image captured by the sensor. The surface is adjusted to better fit the captured image until it converges to the solution.

Klein (KLEIN, 1992) proposed an approach to reconstruct corneal surface based on

Figure 2.11: Eye Netra.

The image illustrates how NETRA is used. The subject looks through a clip-on attached to the smartphone and aligns two lines. After that, the system shows the estimated refractive errors.

Figure from (PAMPLONA et al., 2010)

Figure 2.12: *Arc-step* algorithms steps.

The image illustrates the steps used in the *Arc-step* algorithm in order to estimate the corneal surface.

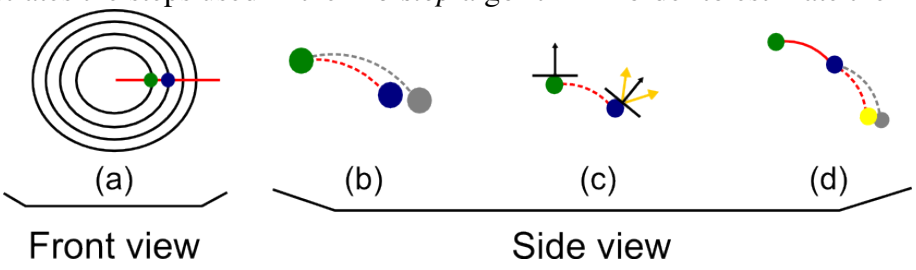

the arc-step algorithm, that produces continuous curvature, which was a problem in previous work (DOSS et al., 1981). The standard algorithm generates discontinuities because it approximates the corneal curvature by a set of individual arcs, causing the discontinuities. Klein's technique approximates each arc using a polynomial of degree 3, instead of 2. Hence, the transition between the two arcs will be smooth.

In a subsequent work, Klein (KLEIN, 1997) discusses the skew ray error during the corneal surface reconstruction and proposes a method to reconstruct the surface avoiding the problem. The skew ray error makes the rings be miss associated and affects the reconstruction. To solve the problem, he calculates the corneal slope and performs adjustments to improve the reconstruction.

Rand et al. (RAND; HOWLAND; APPLEGATE, 1997) claims that the rings pattern cannot be used to reconstruction all types of corneal surfaces. They show a case of corneal surface where they demonstrated that Placido's ring pattern produces an incorrect result. To solve this problem they include radial lines to the standard circular pattern.

2.4 Quality Enhancement and Modeling

Vila et al. (VILA et al., 1995) proposed a robust technique to label the Placido's rings from corneal images. The first step in their algorithm is transform the image into polar

coordinates. This way, the circle will be transformed into near straight-lines. Next, the local maximal pixels are found and classified as ring pixels. After this identification, there might be some discontinuities. To solve this problem, they use a graph approach where the selected pixels are the vertices and the edge costs are given by the pixels intensity and neighborhood information. Finally, a graph search algorithm is used to connect the point in each Placido's ring. Figure 2.13 depicts the process.

Figure 2.13: Connecting discontinuities using a graph search approach.

The image illustrate connecting process. First the rings are transformed to polar coordinates; next the closest graph vertices are connect to connect the lines.

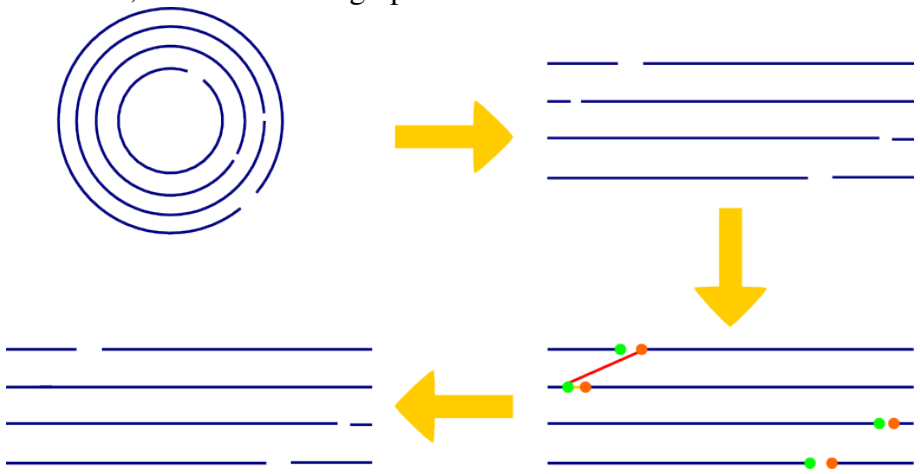

Schwiegerling and Greivenkamp (SCHWIEGERLING; GREIVENKAMP, 1997) used a linear combination, using Zernike polynomials (SCHWIEGERLING, 2004) as base functions, to analyze the values from corneal topographies. Using only the corneal height data it is hard to figure out what the corneal conditions are. The corneal size is much bigger than the size of deviations that cause corneal conditions, complicating the patient diagnoses. To deal with this, one can subtract a standard surface (e.g., a standard cornea) from the height data. Hence, the deviation values become easier to identify. However, we do not have a standard surface to represent all corneal shapes. Another approach to solve the problem is describing the surface as a linear combination of base functions. Using this approach, each base function represents an eye base shape, and the coefficients represent their contributions to the shape of the eye. Schwiegerling and Greivenkamp use Zernike polynomials as base functions, because they form an orthogonal basis function in the unit circle, and can be used to represent corneal conditions. To find the linear combination coefficients, a least square approach is used.

Caneiro et al. (CANEIRO; ISKANDER; COLLINS, 2008) proposed a statistical approach to improve the corneal topography image quality. They divide the image into blocks and perform a statistical normalization for each block, the values are modeled into a normal distribution with zero mean and unit variance. After that, they process these blocks to verify whether the block has interference or not, the interference is noise that affect the Placido's ring detection. A Gabor filter, is used to determine if the block has an orientation. Blocks without orientation is likely to be interference. To detect the orientation into a block, the Gabor filter is applied to different angles as parameters. When one angle has a significantly different value in comparison with the others, the block has an orientation. Next, the mean and standard deviation from all Gabor filters in each block are calculated. A higher standard deviation means higher orientations. A histogram

with the normalized orientations is generated, normally it has a bimodal distribution. The first mode represents interference areas and the second oriented blocks. An expectation-maximization algorithm is used to estimate the means and standard deviations for these two distributions. A threshold based on these parameters is used to remove the interference blocks from image. Figure 2.14 shows the process steps.

Figure 2.14: Statistical approach to improve the corneal topography steps.

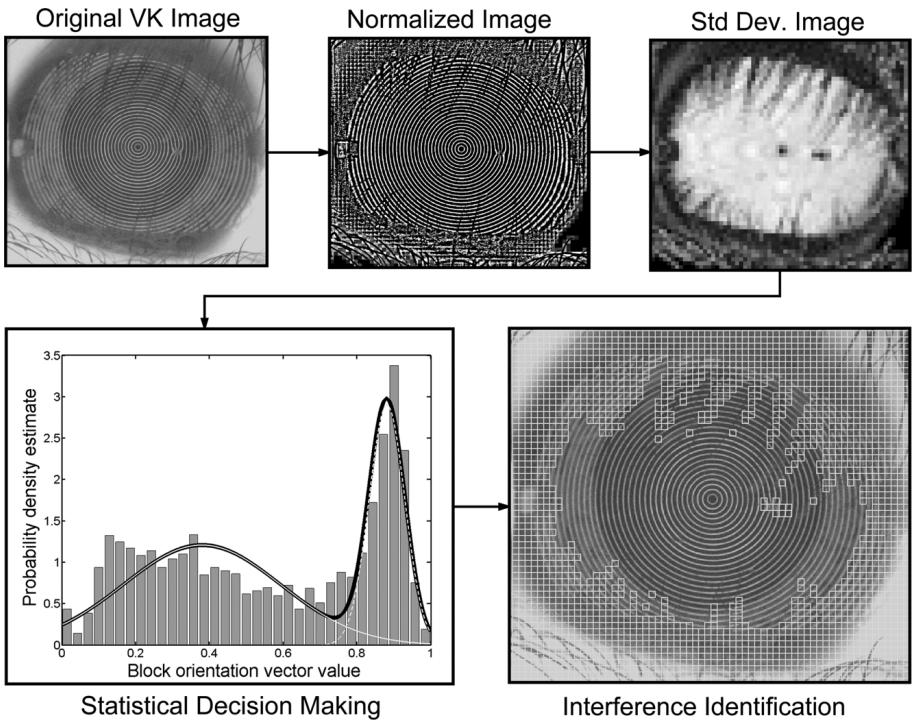

Figure from (CANEIRO; ISKANDER; COLLINS, 2008)

Alkhaldi et al. (ALKHALDI et al., 2009) start to process the image by detecting the centroid of the concentric circles. The algorithm searches a subimage with a complete circular region, calculating objects eccentricity. Then the centroid is calculated using the region geometric center. This point is used to convert the image to polar coordinates, hence the quasi-circular pattern becomes a quasi-straight lines. An adaptive filter is used to improve image quality reducing Gaussian-like noise and also preserving edges. For this task, the pixelwise adaptive Wiener filter (LIM, 1990) is used. After that, a morphological close operation is applied to the image. Finally, the image is converted to Cartesian coordinates. The steps are presented in Figure 2.15.

In this chapter we presented several commercial topographers, we can see that there is an effort to produce smaller and more mobile equipment. These are the same characteristics that our topographer aims, besides the low cost. We saw that ophthalmological exams could be done using smartphones, and it seems a future direction for researches. We presented algorithms to transform the captured images from corneal topographers into corneal surface estimation. Finally, we shown techniques to support corneal topographies: image enhancement algorithms to improve captured images; and approaches to analyze the surface, the Zernike polynomials.

Figure 2.15: Steps of Alkhaldi et al. (ALKHALDI et al., 2009) enhancement procedure for corneal topography images.

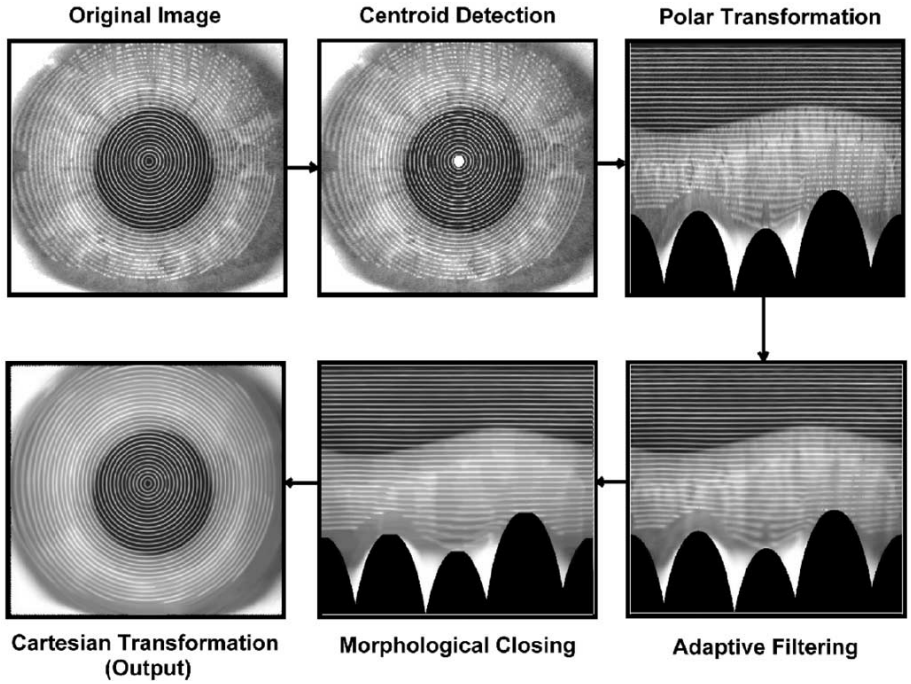

Figure from (ALKHALDI et al., 2009)

3 HUMAN EYE AND CORNEAL TOPOGRAPHY

In this chapter we present necessary concepts for the understanding of the remaining chapters. After discussing the cornea, we conceptually describe how it can be measured. These measures are important for ophtalmologic use. Moreover, we also discuss about Zernike polynomials. They are useful to analyze the data produced by the topographer. We introduce the polynomials and show how to use it from acquired data.

3.1 Human Eye

The human eye is an optical system, that focuses light from the ambient on the retina. Each eye has two lenses: cornea and crystalline. The cornea is a lens with a fixed optical power and it has roughly two-thirds of the total eye optical focusing power (SCHWIEGERLING, 2004). The crystalline, on the other hand, adapts its focusing power to each situation to correctly focus the scene. This process is called accommodation, and it is done contracting or stretching the crystalline. These two lenses focus light on the retina, and especially on the fovea, retina's region with better visual acuity. Figure 3.1 shows an overview of the eye‘s optical system.

To better understand how these lenses affect the vision, we will review the refraction concepts. The Snell's law describes the light refraction when light passes through an interface between two media. It is defined as (Figure 3.2)

$$\sin\theta_2 = \frac{n_1}{n_2}\sin\theta_1 \tag{3.1}$$

where θ_1 is the angle between the incident ray and the surface normal; θ_2 is the refraction angle between the refracted ray and the surface normal; n_1 and n_2 are the refraction indexes from the media. Figure 3.2 ilustrates a light ray refraction.

Using such concepts, we can understand how the cornea works. The cornea's curvature changes the surface normal, that also changes the light path and the point where the light focus. In other words, the visual acuity depends on the corneal shape. Common conditions like myopia and hyperopia are caused by bigger or smaller curvatures than normal. Astigmatism is caused by different curvatures among the meridians. In addition, high-order conditions, such as keratoconus, are caused by irregular corneal curvature (NAKAGAWA et al., 2009).

With this in mind, we can figure out the importance of knowing the corneal topography; mainly in high-order aberrations, where a map showing the differences all over the cornea is useful. This way, due to the corneal shape importance, approaches to perform a corneal topography are developed. Next, we introduce the necessary concepts to understand how to estimate the topography, using a Placido's disk based on approach .

Figure 3.1: The human eye.

This is an optical system with two lenses, the cornea and the crystalline; and a surface that captures the light information, the retina; the fovea is the retina's region with best visual acuity.

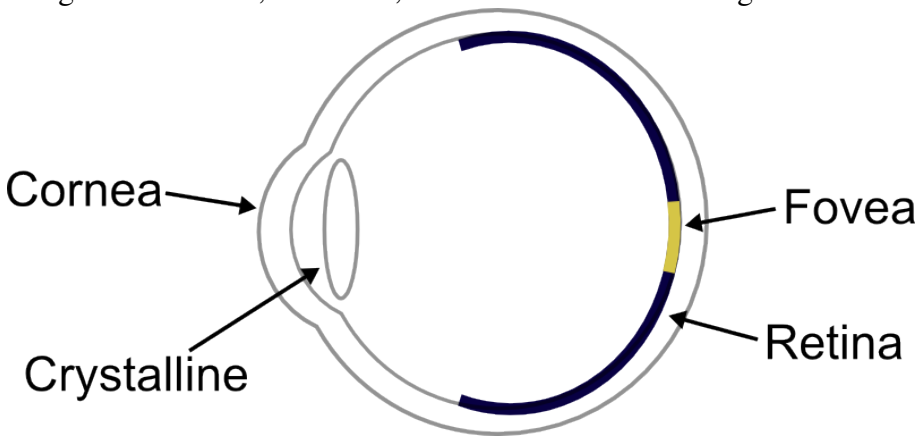

3.2 Corneal Topography Fundamentals

The corneal shape is important to our vision, since changes in its shape imply changes in the visual acuity. There are several approaches to estimate the corneal surface, such as Placido's disks, triangularization methods, and inteferometry (KLEIN, 2000); each one with their characteristics. Due to our focus in this work, I will focus in the approaches based on Placido's disk.

We can summary the corneal reconstruction process using Placidos's disk in some steps. The first one is capture an image of the eye with the reflected patterns. To achieve this, we also need to emit this pattern. After the capture, we start the image processing step. This step consists of identifying the reflected patterns in the captured eye image. We can also use image enhancement algorithms to improve the pattern extraction. From this captured image the pattern borders are identified. Using this border information, we associate the image borders with borders in the emitter. This way, we have the information to estimate the corneal surface. An algorithm is applied to find an approximated corneal surface. Finally, we can also fit the surface with polynomials to get a more compact description and, using the right polynomials, decompose the surface in their optical influences. The process would be summarized in the follow steps: image capture from reflected concentric rings on subject's eye; image processing for feature extraction; and surface estimation using reconstruction algorithms.

The first step in the process is to capture a corneal image. The reconstruction is based on how the cornea reflects light. The pattern captured in the image is from specular reflections. This fact is important because this reflection type follows the law of reflection. The law of reflection says that the angle between the reflected ray and the surface normal is equal to the angle between the reflected ray and the surface normal (see Figure 3.3). From this law, we can see that surfaces with different normals will reflect the incident rays differently. When we capture the image we know where the emitter is and where the light ray reaches the camera. Hence we can use this information for corneal reconstruction.

In the Placido's disk approach, the camera is placed in the middle of the circular pattern, and aligned with the eye center. In this configuration, eyes with regular corneal curvature produce circles in the captured images. Corneas with astigmatism, with different curvatures, produce ellipses. Other conditions, such as keratoconus, produce more

Figure 3.2: Light refraction between a medium interface.

A incident light ray passing through the interface is refracted according to the incident angle θ_1, and the refraction indexes n_1 and n_2. The refraction angle θ_2 can be calculated by using the Snell's law: $\sin\theta_2 = \frac{n_1}{n_2}\sin\theta_1$.

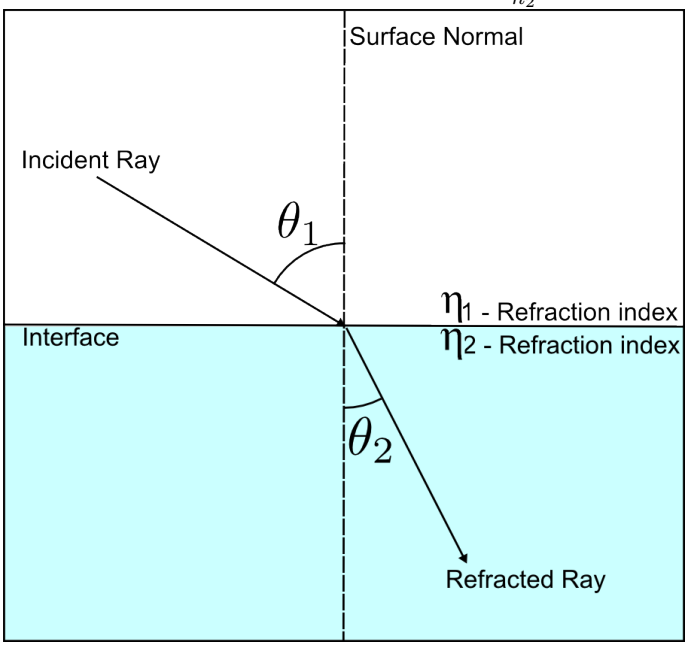

deformed rings. Such an image provides some information about the subject's eye. To capture the image, we need a pattern emitter and a camera; we also need to put them in a correct configuration. The camera is placed in the circle center behind the pattern emitter, in a way where it can capture an image from the cornea. Given that configuration, the subject's eye is placed in a correct distance and a cornea image is captured to perform the exam.

After capturing the image, we start the image processing step. In this step, the pattern is identified in the image and associated with the rings in the emitter. To improve the identification, we can enhance the image using techniques to equalize image brightness, remove noise, and close holes in the pattern or split incorrectly connected rings, for instance. After this, the borders can be identified more easily and correctly. A standard border detector algorithm, such as the Canny edge detector, can be used to detect the borders. Finally, each identified border in the captured image is associated with a border in the emitted pattern. A simple approach to do this is counting the border position from the image center. It is also important to handle cases where the border has some discontinuities, or a noise border that could cause association errors.

After extracting image information and associating it with the emitted pattern, we start the surface estimation step. First, we calculate the angle between the borders pixels and the camera center (Figure 3.4). Hence, we have a vector with the incoming direction from the reflected light ray. We also have the origin position from each emitted pattern, and their order. Using this information, we need to discover a surface that approximately generates a reflection coherent to the data, following the law of reflection. To discovery this surface, we can guess a point position and slope, related to previous calculated points, and iteratively adjust the initial guess. After doing this with each sample from the borders we have an estimated surface. Note that the initial points need special treatment, since we do not have information about previous point — see Algorithm 1. Further details are

Figure 3.3: Law of reflection.

The law of reflection says that in a specular reflection the angle between the incident ray and surface normal is equal to the angle between the reflected ray and the normal. The image shows a visual representation of the law.

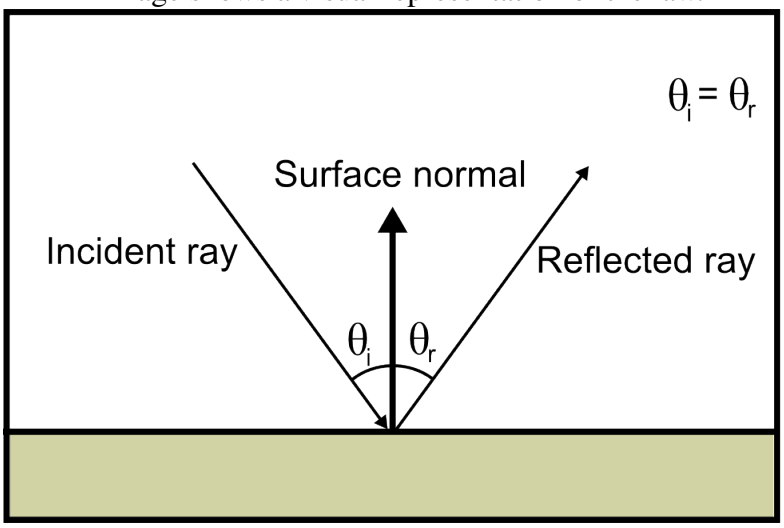

Figure 3.4: Trigonometric relations inside the camera.

The image illustrate the variables used to calculate the trigonometric relation $\tan\theta = \frac{h}{w}$.

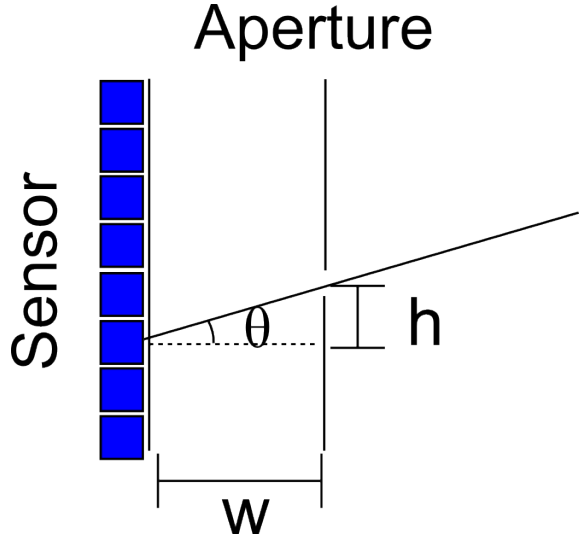

provided in Section 4.2.3 and in (DOSS et al., 1981; KLEIN, 1992).

3.3 Corneal Modeling and Decomposition

Given an estimated corneal surface, we may use a set of polynomials to fit these data to get a compact surface representation. Moreover, the polynomials may identify the contribution of each aberration type in the cornea. To achieve this, we can use the Zernike polynomials, commonly used in optical applications. In this section, we present the polynomials, and also show how to calculate them from corneal samples. Finally, we discuss the optical meaning of each basis function.

Algorithm 1 Surface Reconstruction

```
for each meridian do
  set default value to first sample
  for each other sample do
    repeat
      guess a point
      calculate if it fits restrictions
      if not fit restrictions then
        adjust point
      end if
    until point fit restrictions
  end for
end for
```

3.3.1 Zernike Polynomials

Zernike polynomials are orthogonal polynomials usually defined in the unit disk (NOLL, 1976). They are used in applications where information is encoded in a circle, which is common in optics applications due to the use of a circular aperture. Using these polynomials, captured data can be represented with few parameters, also each polynomial has a specific meaning to help data analysis. To understand how to use these polynomials, we need to understand first, how they are defined and combined; second, how to get the polynomials coefficients from captured data; and, finally, what their meanings are.

Zernike polynomials are defined using a double index, representing radial and angular components. Their definition

$$Z_n^m(\rho,\phi) = \begin{cases} N_n^m R_n^{|m|}(\rho)\cos(m\phi), \text{if } m \geq 0 \\ N_n^m R_n^{|m|}(\rho)\sin(m\phi), \text{if } m < 0 \end{cases} \tag{3.2}$$

can also be divided into radial ($R_n^{|m|}(\rho)$) and angular parts ($\cos(m\phi), \sin(m\phi)$), and a normalization factor (N_n^m) that is not always included. The radial factor is defined as

$$R_n^{|m|}(\rho) = \sum_{s=0}^{(n-|m|)/2} \frac{(-1)^s (n-s)!}{s![0.5(n+|m|)-s]![0.5(n-|m|)-s]!}\rho^{n-2s}. \tag{3.3}$$

The angular part is $\cos$, if m is a positive value, or $\sin$ if it is negative. Note that the value m used in the equation is always positive. The normalization factor is used to transform the polynomials into orthonormal, but a convention to use it, or not, does not exist. It is defined as

$$N_n^m = \sqrt{2(n+1)/1+\delta_{m0}} \tag{3.4}$$

where δ_{m0} is the Kronecker delta function, defined as

$$\delta_{m0} = \begin{cases} 1, \text{if } m = 0 \\ 0, \text{otherwise} \end{cases}. \tag{3.5}$$

A visual representation for the polynomials is presented in Figure 3.5.

Figure 3.5: Zernike polynomials.

The image shows different polynomials ordered by the radial index vertically and by the angular index horizontally. The color represents the function values, blue is one and red is minus one.

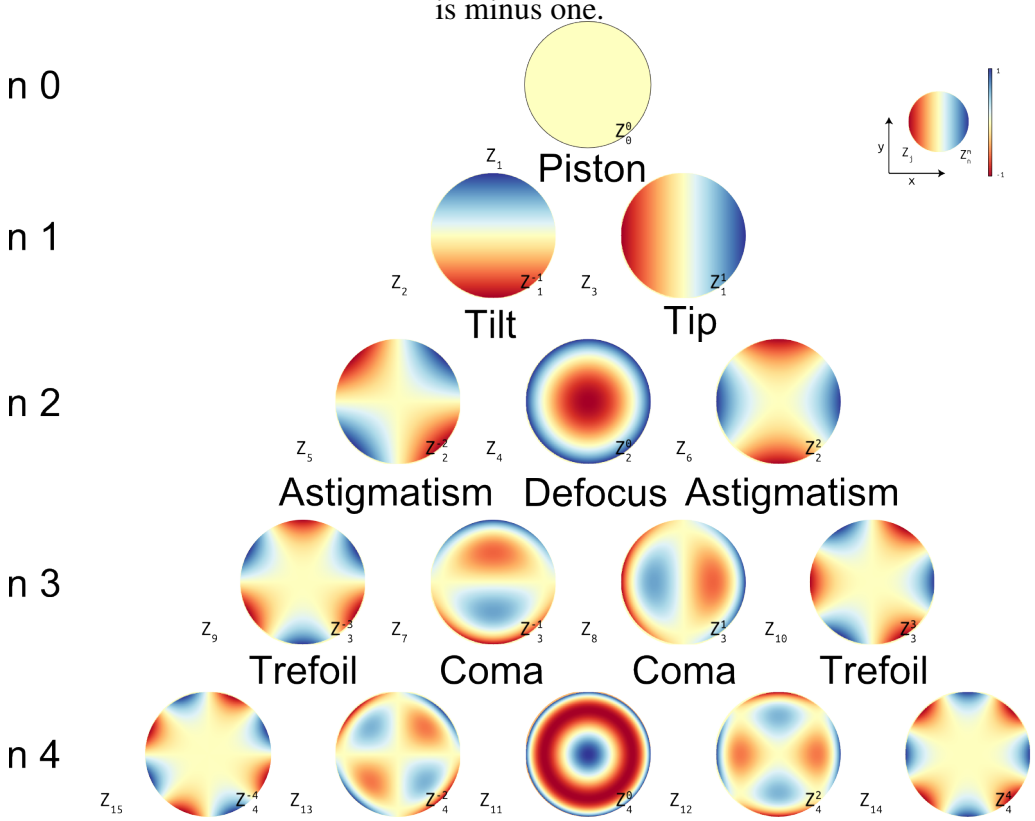

Image adapted from: (COMMONS, 2013a)

To build complex surfaces, the polynomials are linearly combined. In the continuous domain, a surface can be represented using an infinite series of polynomials, or approximated by a finite numbers of terms. These equations can be written as

$$S(\rho, \phi) = \sum_{n,m}^{\infty} c_{n,m} Z_n^m(\rho, \phi) \tag{3.6}$$

or in the approximated case

$$S(\rho, \phi) \approx \sum_{n,m}^{N} c_{n,m} Z_n^m(\rho, \phi). \tag{3.7}$$

They can also be written in matrix form

$$\begin{bmatrix} x_1 \\ x_2 \\ \vdots \\ x_n \end{bmatrix} = \begin{bmatrix} Z_{0,0}(\rho_1, \phi_1) & Z_{1,1}(\rho_1, \phi_1) & \cdots & Z_{n,m}(\rho_1, \phi_1) \\ Z_{0,0}(\rho_2, \phi_2) & Z_{1,1}(\rho_2, \phi_2) & \cdots & Z_{n,m}(\rho_2, \phi_2) \\ \vdots & \vdots & \ddots & \vdots \\ Z_{0,0}(\rho_n, \phi_n) & Z_{1,1}(\rho_n, \phi_n) & \cdots & Z_{n,m}(\rho_n, \phi_n) \end{bmatrix} \begin{bmatrix} c_{0,0} \\ c_{1,1} \\ \vdots \\ c_{n,m} \end{bmatrix} \tag{3.8}$$

or in a compact form

$$\vec{x} = Z\vec{c} \tag{3.9}$$

Figure 3.6: Coma and astigmatism polynomials represented in 3D.

The first row shows a coma visual representation. The second row illustrates an astigmatism polynomial.

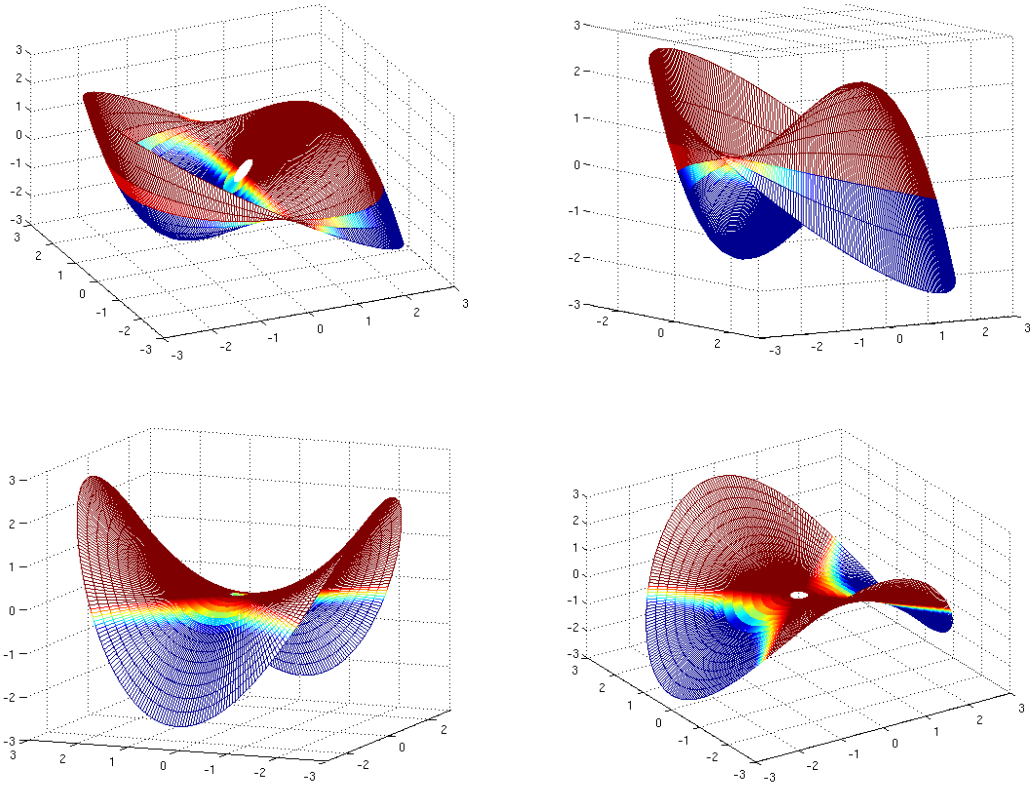

where Z is a matrix with polynomial values; $\vec{c}$ is a vector with linear combination factors and $\vec{x}$ is a vector with surface values.

3.3.2 Using the polynomials

In practical applications, we have samples of a measured object, with a value for a radius and an angle. Putting these values in Equation 3.8 we can obtain the matrix Z (using the angle and radius to evaluate the individual polynomials — Equation 3.2) and the vector $\vec{x}$ (the sampled values). The $\vec{c}$ coefficient vector is unknown. This way, we need to solve Equation 3.9 for $\vec{c}$.

$$\begin{aligned} Z\vec{c} &= \vec{x} \\ Z^{-1}Z\vec{c} &= Z^{-1}\vec{x} \\ \vec{c} &= Z^{-1}\vec{x} \end{aligned} \tag{3.10}$$

To solve this equation we need to calculate the Z^{-1}, but, normally, the number of samples is bigger than the number of polynomials and coefficients. This means that to solve the equation for the coefficients $\vec{c}$ an inverse matrix cannot be used. A common approach is to solve the equation using the method of least squares. First, Equation 3.9 is multiplied by their transpose in both sides

$$Z^T Z\vec{c} = Z^T\vec{x}, \tag{3.11}$$

and, finally, we can solve for $\vec{c}$

$$\vec{c} = (Z^T Z)^1 Z^T\vec{x}. \tag{3.12}$$

Table 3.1: The first Zernike polynomials and their respective names. The polynomials are identified by their different indexes.

Radial Index (n)	Angular Index (m)	Polynomial	Name
0	0	1	Piston (mean value)
1	-1	$2\rho \sin\theta$	Tilt
1	1	$2\rho \cos\theta$	Tip
2	-2	$\sqrt{6}\rho^2 \sin 2\rho$	Astigmatism
2	0	$\sqrt{3}(2\rho^2 - 1)$	Defocus
2	2	$\sqrt{6}\rho^2 \cos 2\rho$	Astigmatism
3	-3	$\sqrt{8}\rho^3 \sin 3\rho$	Trefoil
3	-1	$\sqrt{8}(3\rho^3 - 2\rho) \sin\theta$	Coma
3	1	$\sqrt{8}(3\rho^3 - 2\rho) \cos\theta$	Coma
3	3	$\sqrt{8}\rho^3 \cos 3\rho$	Trefoil

Solving the equation, we get the coefficients to a surface that best fit the input data. These coefficients have special optical meanings. Each coefficient represents the amount of the optical aberration in the fitted surface. This is important for analyzing the surface. Table 3.1 shows a list of the first polynomials and their optical meanings. A useful example, for corneal analysis, is the coma coefficients ($n = 3$, $m = -1$ and 1), which are associated with keratoconus. In other words, if a subject has keratoconus, the coma coefficient has greater magnitude. A 3D visual representation of a coma and an astigmatism polynomial is present in Figure 3.6, In this representation, both coefficients are equal to 1.

3.4 Summary

This chapter presented the fundamentals that we need to understand the rest of this thesis. In relation to corneal reconstruction, it presented the basic steps to corneal reconstruction using the Placido's-disk approach: image capture; image enhancement and rings extraction; and finally, the corneal surface estimation. The chapter also discussed corneal modeling using Zernike polynomials.

4 BUILDING A CORNEAL TOPOGRAPHER

So far we have discussed the topographer fundamentals and the corneal-surface estimation process used in approaches based on Placido's disk. We have implemented a corneal topographer prototype based on a cell phone camera and a clip-on device, whose concept is depicted in Figure 4.1. We have used this prototype in conjunction of the pipeline described in the Section 3.2. From the captured image, we apply an enhancement process to extract the necessary information from the image. It is important to note that our prototype focuses on cost and construction simplicity. During the image processing step, the borders are sampled and associated to the borders in the pattern. At this point, we use an algorithm to find incoherences in the association step, and also solve these incoherences. Finally, we use the extracted information to estimate a corneal surface. We use an iterative algorithm that approximates each point pair, in a meridian, by an arc, using the law of reflection. From such arcs, the surface of the entire cornea is estimated.

This chapter is organized as follow. First, the hardware model and its implementation presented (Section 4.1). Following, algorithms for processing the captured image and extract the reflected rings are presented in Section 4.2. Finally, Section 4.2.3 discusses reconstruction methods for cornea surfaces from placido's rings.

4.1 Hardware

To perform corneal surface reconstruction, first we need a device to capture the reflected rings on the cornea. We use the cell-phone camera to capture the cornea image. Our pattern was developed to allow the capture of a corneal image with the camera placed at the center of the rings (Figure 4.1). Also, we look for a device simple to be built. This section shows our device implementation. First, we describe a conceptual model, then we present how we have implemented it.

4.1.1 The Conceptual Model

It is important to note that the emitter needs to be placed in a way where the pattern could be reflected and captured by the camera. In face of that, we build a clip-on device with three layers. The first one, the *illumination layer*, provides the illumination; the second one is used as a *support layer*, helping with the image captured using a lens and also with the light diffusion; the last layer is used as the pattern layer, and is responsible to give the shape to the pattern. These layers are put together and attached to a cell phone 4.1.

Our prototype was developed around the pattern emitter; it was built in a way that allows the cell phone to be attached and capture an image from the cornea. The first layer

in the pattern emitter is the illumination layer. The attenuation layer, with the concentric circles, is placed between the illumination layer and the cornea, in a way to correctly project the pattern on the cornea. While most topographers have conical, spherical, ellipsoidal or cylindrical forms to increase the area measured (JONGSMA; BRABANDER; HENDRIKSE, 1999), we have used a flat surface to simplify the manufacturing of the device. These layers have a hole in their center, through which the camera captures the corneal image with the reflected pattern.

The support layer is used to attach a lens to improve image focus at close distance, and zoom in (enlarge) the corneal region. The lens is placed at one focal distance from our camera, hence the light rays reaching the lens parallel to the system's optical axis are focused at the camera lens center. The device configuration is shown in Figure 4.1. The support layer has also another function, diffuse the illumination provided by a set of LEDs.

In summary, our light emitter has three layers: the first one provides illumination for our device; the second one acts as a diffuser and also supports a lens to improve the image captured; and finally, the third layer that is responsible for the pattern projection. These layers are aligned and have holes in at their centers, through which the camera can see the reflected pattern on the corneal surface. Next, we present the prototype's implementation details.

4.1.2 Prototype Implementation

The back illumination is provided by an electronic board with 36 LED's, arranged as a 6 by 6 grid. Our board has 10x10cm, we use 3 volts LED's using a 12 volts power supply, hence we use 9 set of 4 LED's connected in series. A hole with 5mm was cut at the center of the board to capture the cornea image. On top of that, an acrylic layer with diffuse paper is placed to diffuse the LED illumination and a lens to improve the image capture. Finally, another acrylic layer (the support layer) is placed with the pattern (the pattern layer - a set alternating black and transparent concentric circles) printed on a transparent layer (acetate). For the prototype we uses 14 transparent concentric disks, each with width 3 mm. An additional layer of diffuse paper was also added to improve light diffusion. The support and pattern layers also have holes in their centers, in this case with a diameter of 1cm. The reference distances to our clip-on prototype is presented in Figure 4.2. The clip-on was tailored to Nokia N900 cell phone (NOKIA, 2013), the cell phone that we use in this work.

To capture the cornea image, the support layer has a lens to improve the captured image. This lens is one focal distance, 45mm in our implementation, from the camera lens. To avoid influences from the back illumination, two components were added to the device. First, an ethylene vinyl acetate (EVA) sheet was placed behind the electronic board because our board has holes where the light pass through reaching the camera interfering in the image processing. And a pipe was placed between the electronic board and the middle layer. Hence, we can capture a image from the cornea.

To put all these together, acrylic parts are used. Behind the prototype, a piece was placed to fit the cell phone so that it will be aligned with the holes. In the front, a base to support the subject's forehead is placed to achieve correctly focused images. A photograph of the actual clip-on device prototype is shown in Figure 4.3. Finally, we describe a device to capture the images from a pattern emitted into the cornea. Next, we discuss how to estimate a corneal surface from the information captured with the prototype.

Figure 4.1: Conceptual prototype model.

Our device model is composed by three layers: the first provide illumination for pattern projection; the second is used to better diffuse the emitted light, and is also used to place a lens to improve image capture quality; the last is used as attenuation layer, this layer is responsible to define the emitted pattern. A perspective visual representation of our prototype is shown in (a), a side view is present in (b).

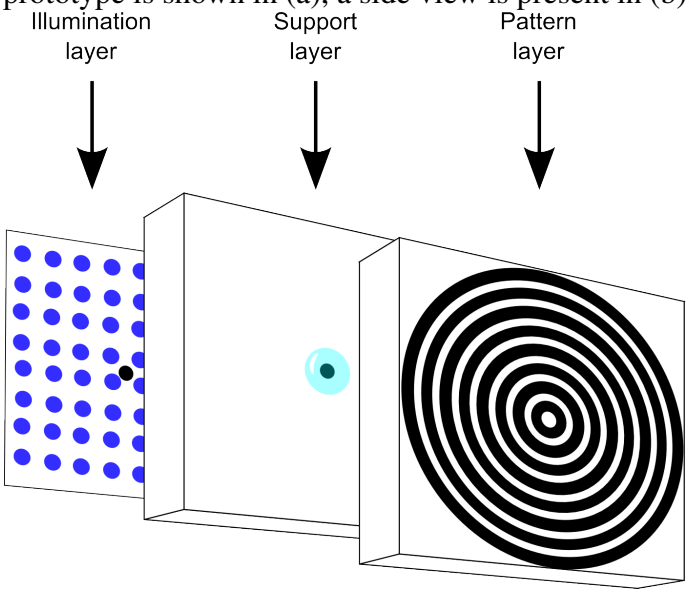

(a) Prototype model

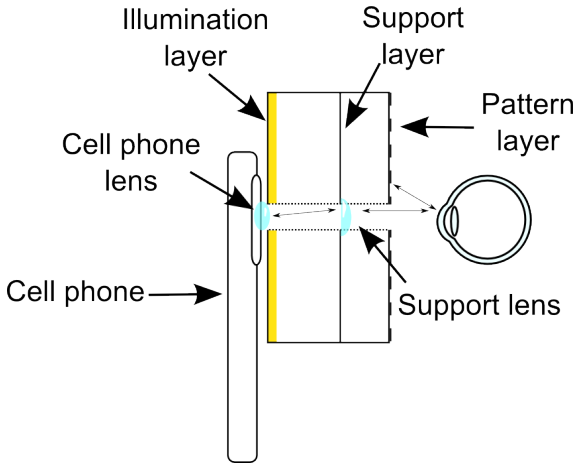

(b) Plain prototype model

4.2 Algorithms

After capturing an image of the projected pattern , the image is transferred from the cell phone to a personal computer, where it is processed to estimate the corneal surface. First, we need to extract these patterns. This is done using a sequence of image processing algorithms, to enhance image quality and extract the patterns. From the extracted patterns reflected onto the cornea and the knowledge about the reflected pattern, an iterative algorithm is used to estimate the subject‘s corneal surface. We implement all algorithms using MATLAB. These algorithms are described next.

Figure 4.2: Clip-on prototype distances diagram

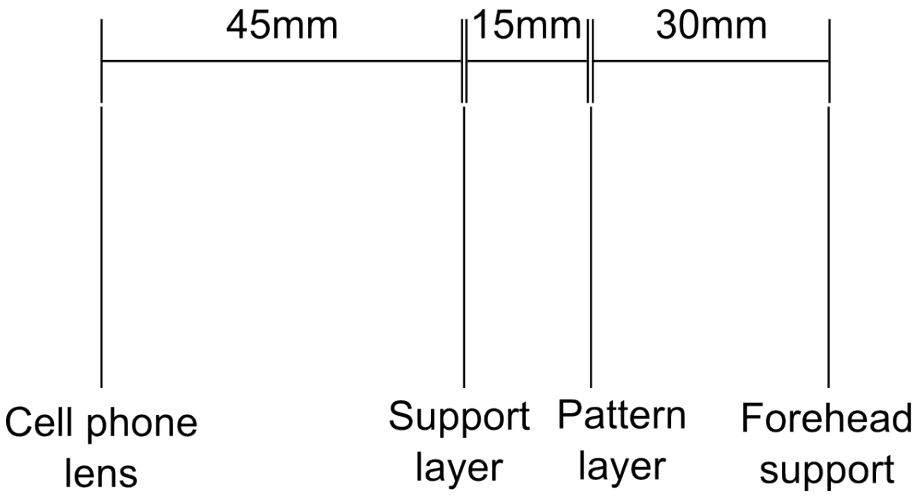

Figure 4.3: Clip-on device prototype

Actual clip-on device prototype comprising three layers: illumination, attenuation, and pattern layers. A general view is presented in (a) and (b). All the equipment used in image capture is presented in (c). We show the clip-on with the cell phone in (d). A clip-on device side view is presented in (e). And (f) illustrate a examination.

(a)

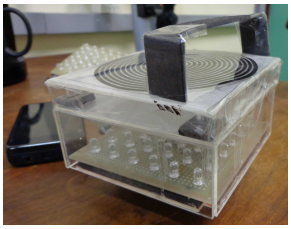

(b)

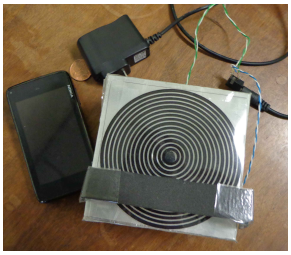

(c)

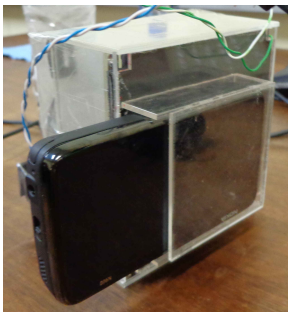

(d)

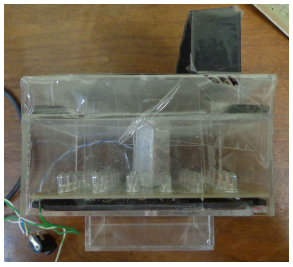

(e)

(f)

Figure 4.4: Captured Image.

Our prototype captures an image in a region larger than the eye region. The eye is placed at image center, our interest region. In the other regions, the camera captures images from the prototype.

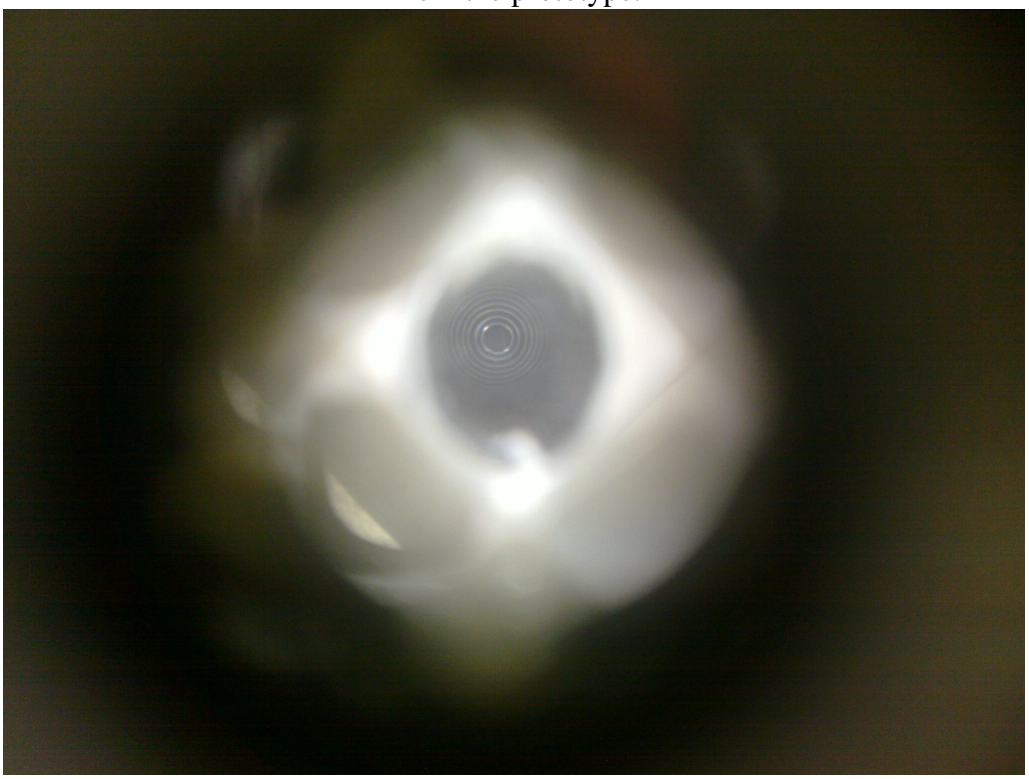

4.2.1 Image processing

At this point in the reconstruction process, we have a captured image from the Placido's disk pattern. The captured image has several irrelevant regions to our process (see Figure 4.4). Moreover, the contrast between the patterns and the eye is very low. With improvements, this images can, more easily, be used to compute an estimate of the corneal surface.

To automatically estimate the corneal surface. We need to associate each border in the captured image with a ring from the emitted pattern. For this, we need to identify the pattern in the image, in other words, we need to segment the pattern in the image. To improve the final result, the segmented rings can be enhanced to produce sharper borders to simplify the detection step.

To perform those tasks, we use an image processing algorithms pipeline. First, we find the eye centroid and crop the region around it. After that, we stretch the image contrast and correct the image lightness using morphological algorithms. Next, we extract the patterns using differences of Gaussians. Finally, the resulting image is enhanced to simplify border detection. Next, we discuss each step in detail.

Our prototype captures an image with an eye in the center and prototype parts in the sides. Thus, we need to find the eye center in the image and crop an area around this point. To identify the eye center we search for the innermost ring center. The problem is that we do not know the exact ring position, size (radius), nor its shape. We use a cross-correlation operator to find its center. The operator centralizes a circular kernel and performs a weight average using the kernel values as weights. We use a circular

kernel, in other words, we count the number of points in the circle defined in the kernel. Hence, the pixel with the greater values is at the center of a more defined circle. This operator is used only in the image's central region, to avoid inappropriate identifications. To validate this procedure, we used a set of images captured from normal eyes and eyes with keratoconus, and identified the center manually and automatically. We compare the values and the difference is about 1 or 2 pixels, which we classify as acceptable. The result from the cropping procedure is shown in Figure 4.5.

Figure 4.5: Cropped image.

Eye with pattern reflected on the cornea, after cropping the eye from the image shown in Figure 4.4.

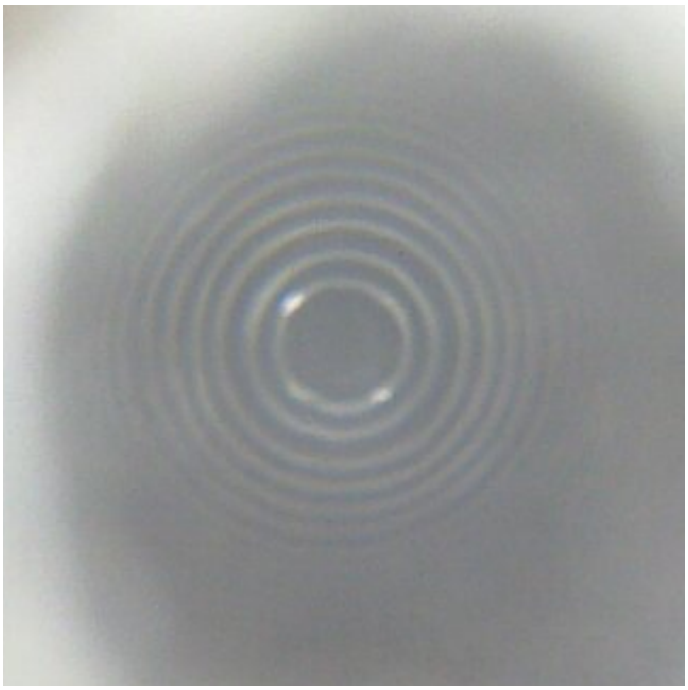

The eye region (Figure 4.5) uses a small color range to represent the eye and the pattern. Consequently, it exhibits low contrast. Thus, we normalize the image, stretching the contrast and helping the next steps in the process. Figure 4.6 presents a normalized image.

After stretching the image contrast, we convert it to lightness. This step simplifies the next steps of the algorithms, since we have applied them to a single channel. Moreover, we do not need the color information for our purpose. We only need the information about the pattern shape. An image converted to lightness values is presented in Figure 4.7. It is important to note that the normalization process is performed before the lightness conversion.

The lightness image has a large bright area, that does not correspond to the pattern. This hampers the rings identification. To deal with this problem, we use morphological operators. First, we use a median filter to remove noise, note the noise in Figure 4.6. After that, we use the top-hat transform (ZHOU; WU; ZHANG, 2010) to remove the irregular background illumination. To perform the top-hat transform, first we apply a morphological opening. The opening operator applies an erosion and dilation in the image. The erosion reduces the objects and removes small objects, the size of this objects is related to the structuring element size. The dilation increases the object sizes, hence the non-removed objects return to their original size. In our case, the patterns are almost removed.

Figure 4.6: Normalized image.

To simplify the emitted pattern extraction, the image is normalized, increasing the contrast.

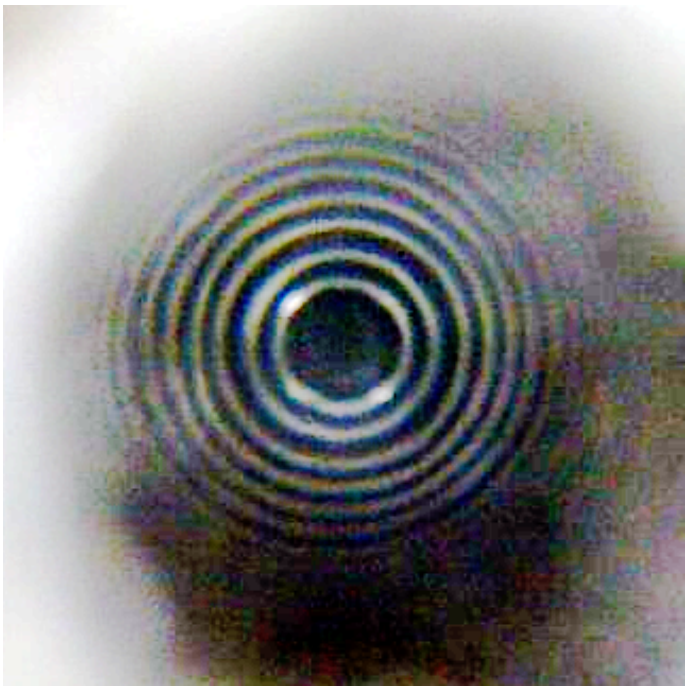

Figure 4.7: Lightness image.

The pattern extraction is simplified using only the lightness image.

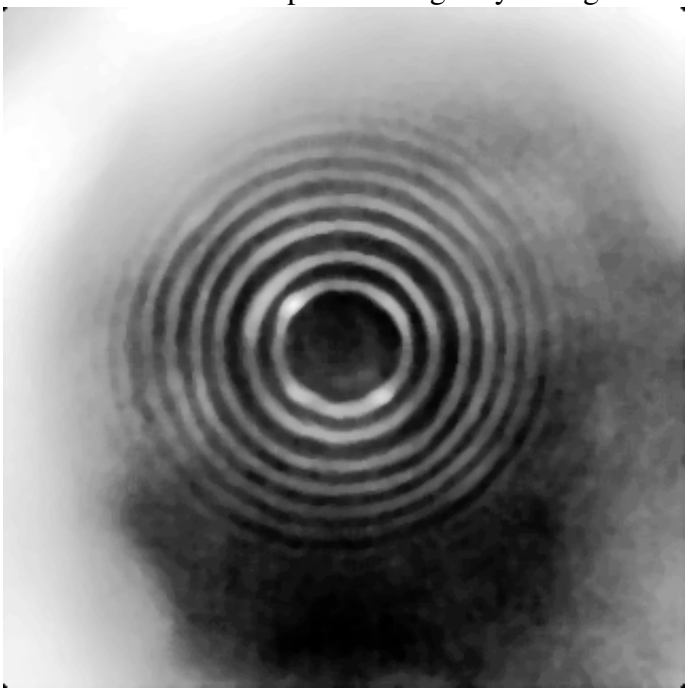

To complete the top-hat transform we subtract the open image from the original. Consequently, we remove it all from the original image, except the removed objects, in our case the pattern. Figure 4.8 shows the results from the top-hat transform application.

In the top-hat transform image, the pattern is well defined. However during our tests it is not enough to our goal. To solve this we use a difference of Gaussians (ACHARYA;

Figure 4.8: Top-hat image.

Result of applying the top-hat transform to the image shown in Figure 4.7.

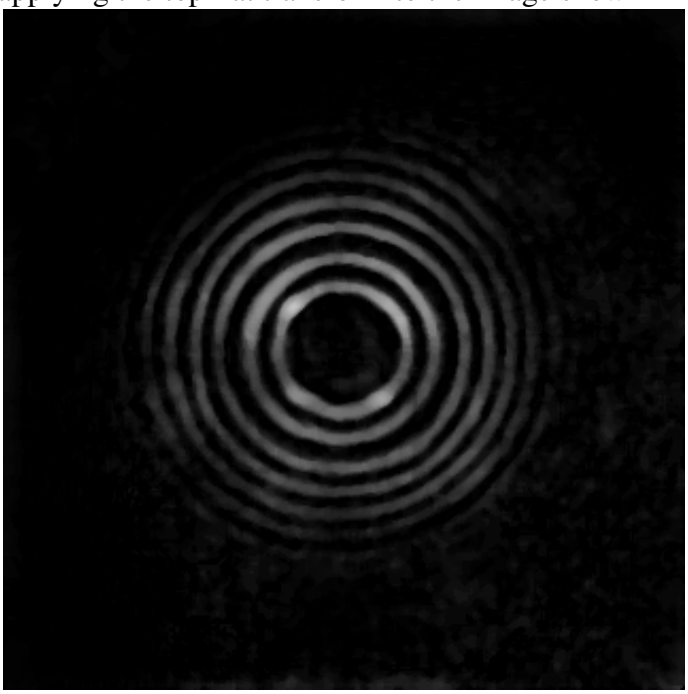

RAY, 2005) twice to extract the pattern. We can see the extract patterns in Figure 4.9. The difference of Gaussians operator approximates the Laplacian of Gaussian, that detects edges and also applies a filter to remove noise from image. We use large Gaussian kernels to identify the pattern as borders. For the differences of Gaussians we use kernels with size 20 and 5 pixels, respectively. Such values were defined empirically.

Figure 4.9: Difference of Gaussians image.

Before detecting the emitter pattern border, we extract the pattern from the image.

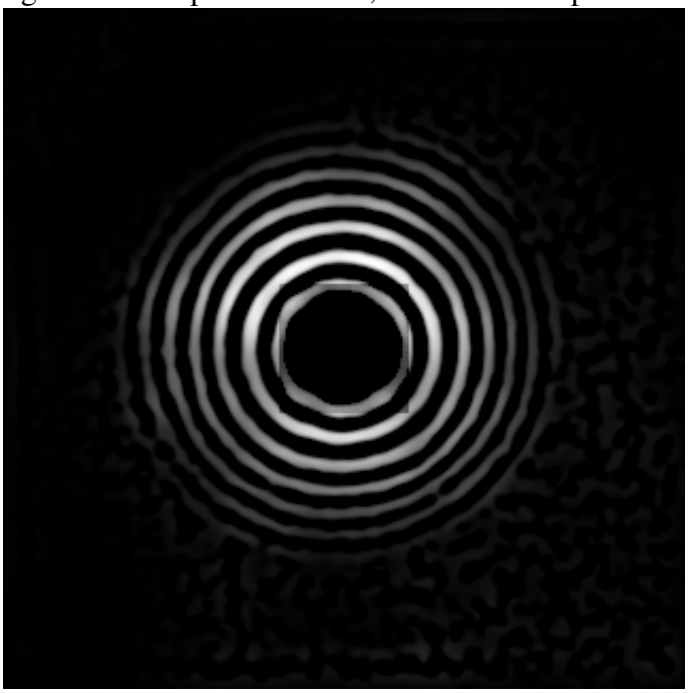

With the pattern extracted, we enhance the image before the reconstruction sampling. A captured image is composed by the real image or signal, what we want, and noise the changes the image, that is undesirable. To try to recover the real image, the Wiener filter uses a statistical approach to minimize the square differences between the recovered image and the real one. We use the Wiener filter to improve our image before extracting the borders. Before appling the filter we convert the image to polar coordinates, hence the circles become near straight lines. Then, we use the Wiener filter with a rectangular kernel, with size 3 by 15 pixels. Such values are also empirically defined. Next, we apply a morphological close operation to the image.

The close operation applies a dilation and an erosion to the image. The dilation operation closes small holes in the image and increases the object borders. After that, the erosion operator reduces the object borders. This way, the image holes is closed and the borders smoothed. Finally, the polar image is transformed into a Cartesian image. Our approach to improve the image is similar to the proposed by Alkhaldi et al. (ALKHALDI et al., 2009). Figure 4.10 shows an image improved by the Wiener filter and the morphological operations.

Figure 4.10: Enhanced image.

The extract pattern is enhanced to improve the border detection.

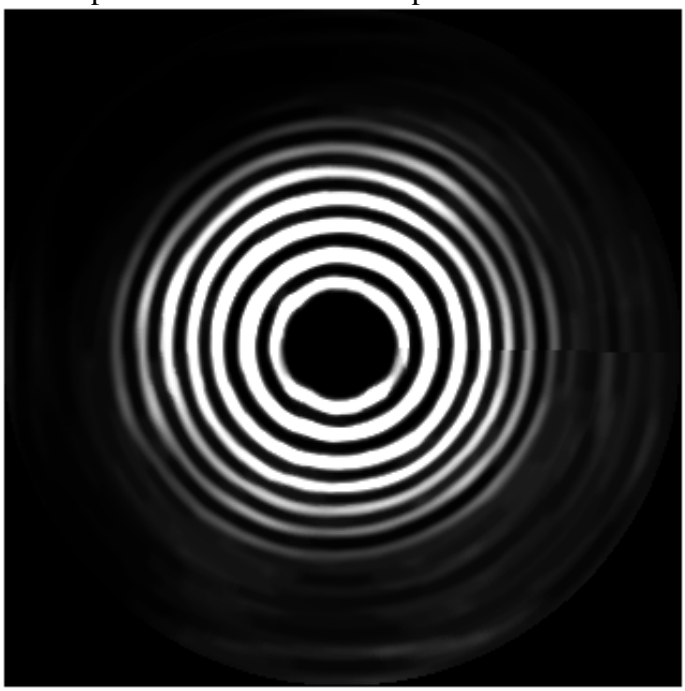

4.2.2 Pattern sampling

In order to reconstruct a cornea surface from the extracted pattern, we need a sampling process. In this process, we link each border between the extracted pattern to a border in the emitter pattern. To achieve this, first we use the Canny algorithm (CANNY, 1986) to detect the extracted pattern borders. There are cases where a border is not detected or an extra border is detected. To solve these situations, we use a connected component voting scheme. After that, we use a graph approach looking for incoherences. Next, we discuss these sampling steps.

The voting scheme begins searching the connected components using standard algo-

Figure 4.11: Borders detected image.

To sample the image, the pattern borders are detected using the Canny edge detector.

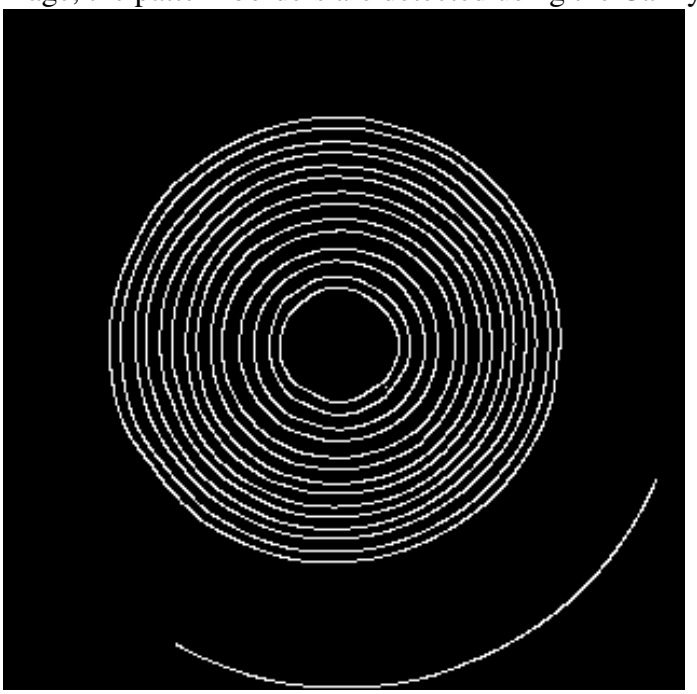

rithms. Each connected component needs to be associated with a ring in the emitted pattern. However, there are cases where two adjacent lines may be connected, in these cases we need to split the connected components in two. To separate them, we develop a split algorithm that we apply to each component. The algorithm begins seeking an end point, that is, one pixel where is not possible to reach other adjacent border pixel apart from the pixel used to reach it. Next, the algorithm walks, using the pixel adjacency, from an end point to a place where the walk direction changes or another end point. To identify direction changes, the current and next pixels in the walk are transformed in vectors with the origin in the image center. The cross product from these vectors is calculated and the sign is compared with the sign in the next step, if the direction changes, the sign also changes. When the direction changes the connected component is split and these two new connected components pass through the algorithm again.

Since we have each connected component from only one ring in the pattern, we need to discover what ring it is. For this, we count the numbers of borders found in the image center in each angle. Hence, each connected component is labeled with a ring index for each angle. We consider each label as a vote for the index related to the component. At the end, we choose the most voted index as the component index, like a common voting process. During this process, we also keep the prior and next connected components for a posterior coherence validation (see Algorithm 2). This validation is discussed next.

We use a graph approach to detect incoherent situations. Our graph is built using the next and prior votes from the previous step. Each connected component is a vertice and the edges are the more voted next and prior connected components. Values are attributed to each edge representing the difference between them, in rings, from the pattern. In a complete correct graph, the values of all edges would be one. However, imperfections in the detected borders and noisy connected components can occur, Figure 4.12 illustrates these situations. In these cases, edges with value zero and more than one may appear in the graph. In the case where the edge has values bigger than one, the value can be

Algorithm 2 Voting and Graph Building

```
for each angle do
    calculate distances for all connected components to eye center
    sort distances
    for index 1 to number of rings do
        votes[distances[index]].cc = index
        calculate if it fits restrictions
        if index > 1 then
            priorVotes[distances[index].cc] = distances[index-1].cc
        end if
        if index < number of rings then
            nextVotes[distances[index].cc] = distances[index+1].cc
        end if
    end for
end for
for each conn componet do
    ringIndex = max(votes)
    graph(ccIdx, max(priorVotes[ccIdx]) = EDGE
    graph(ccIdx, max(nextVotes[ccIdx]) = EDGE
end for
```

Figure 4.12: Sample situations.

The figure illustrates three possible cases of border classifications. First, the normal case (left) with sharp rings, the simplest case to deal. The second case (center) happens when a ring is detected with discontinuities, like in the red, green and blue rings, for instance. Finally, in the last case (right) an extra ring is detected from image noise, like the tiny dark green ring.

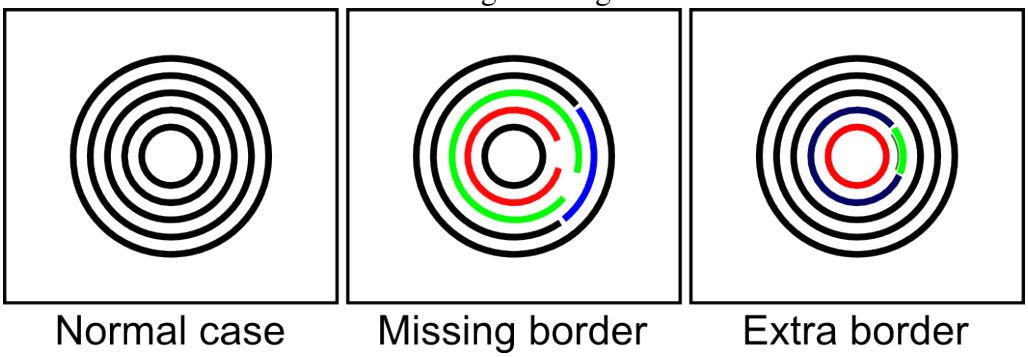

explained by the abscence of one edge in the path. However, when the edge value is zero, the edges are related to the same ring, which is incoherent due to one is after the other (see Figure 4.13). Hence, we have a wrong border classification. When this happens, this error is propagated to the next borders.

Based on these observations, we can use an algorithm to adjust the incoherences. First, we search for egdes with zero value. We assume that the second vertice from the edge with value zero needs to be incremented by one, because during the voting process one increment has been left behind. Hence, we increment this vertice, but it may imply a new incohence if the edges from this vertice has value one. This fact is from the error propagation, hence we also need to propagate the adjusts. In summary, our algorithm

Figure 4.13: Graph incoherences.

The figure illustrates how the incoherence discovery process work. The input image may have a ring configuration that makes the voting process fail. The voting table shows the positions associated with each ring in the example input image. The red, green and yellow rings are in their correct position, however the blue ring is not. We build a graph using the neighborhood information between the rings that says what are the prior and next rings, also from a voting process. The edge values in this graph are calculated using the difference between the two adjacent vertices. Note that the green and blue vertices are subsequent and have a 0 zero distance, this is incoherent.

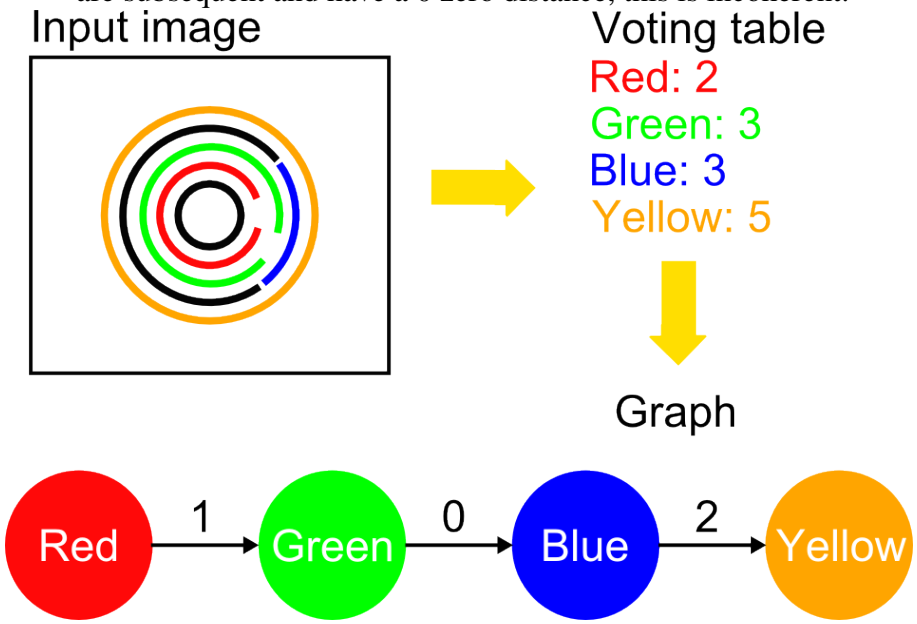

finds the zero edges and adjusts the next vertices until it finds an edge with value bigger than one or the graph ends.

4.2.3 Surface reconstruction

After completing the previous step, we have collected the following information for each sample (pixel in the ring pattern): distance from the center of the eye, angle between the vector from the center of the eye and a vertical line, and the index of the ring to which the sample belongs to. From our device setup, we know that the light rays are parallel when they reach the lens and converge to the center of the captured camera lens – Figure 4.14. Hence, using trigonometric relations, we know the intersection distance between the reference axis, the camera's lens center, and the support lens, Figure 4.15 illustrate these relations. Taking in account that the incoming light rays are parallel to our reference axis, we know the distance the axis to the position where the light reflected in the eye. After use this logic in two dimension we calculate the angle and distance to the reference axis, this way we will work polar coordinates. Now, we need to discovery a height for each sample to estimate the cornea surface. We use the arc step algorithm (DOSS et al., 1981; KLEIN, 1992) approach to achieve this. Next, we discuss the algorithm.

To estimate the samples height, we use two facts: first, the captured pattern is from specular reflection, and follows the law of reflection; second, the eye has a near spherical form. The specular reflection is used to validate if a candidate height, and slope, is correct. The near spherical form is used as a guide to guess candidates and calculate the slopes.

Figure 4.14: Prototype lens scheme.

The first lens, L1, that is placed in the support layer refracts the parallel rays to the center of the cell phone lens, L2. It happens because the distance between the lenses is equal to L1's focal distance. This way the system is focused at infinity.

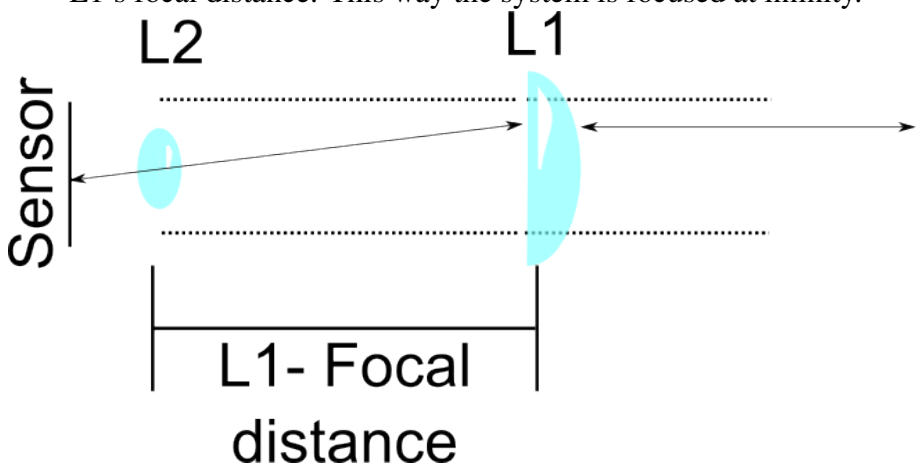

The arc-step algorithm uses three restrictions for a pair of points:

1. The arc between the two points is an arc from a circle;
2. The normal one from the first point remains the same;
3. The calculated surface respects the law of reflection.

These three conditions are sufficient to calculate a unique arc (KLEIN, 1992). Hence, we can check if a point is correct, but we still need to find the correct height.

To find the point value, we use an iterative approach for each sample. Figure 4.16 shows an overview of this process. To respect the above conditions, we also need the value from the previous point. The first point requires special treatment, we set all the old values to zero, and guess a little value to the height. We begin our search with an initial guess. To get a value close to the expected one, we use a Taylor expansion based on the value and derivatives from the previous point. Based on the initial guess and the values from previous iteration, point and slope, a circle passing through the two points and that has the same slope than the previous point is calculated. Hence, we calculate the normal and slope from the guessed point. Figure 4.17 depicts the normal from our point. Next, the angles between the normal and the incident and reflected rays are calculated and compared. When the angles are virtually equal (their difference is smaller than a certain threshold) we accept the point as correct. After calculate all the points we have a estimated surface as shown in Figure 4.18.

4.3 Summary

This chapter described how we have implemented a prototype of the proposed corneal topographer. It covers all the steps from image capture to surface reconstruction. Fist, we introduced our prototype conceptual model and then presented the hardware construction details. We built a clip-on device to be attached to a cell phone that allows us to captures the images with the reflected Placido's disks.

We have discussed how we deal with the captured image in order to perform the corneal reconstruction. First we describe algorithms to enhance the image and segment

Figure 4.15: Trigonometric relationship in the prototype.

In our prototype, we know the value of variables H1, W1 and W2 in the draw. We calculate H1 from the pixel position in the image and the pixel length in the sensor. From camera specification we know W1 and W2 from our device measures. Since H1/W1 = H2/W2, we can calculate H2 = H1/W1 * W2. H2 is the distance between our reference axis and the position where the light reflected in the eye.

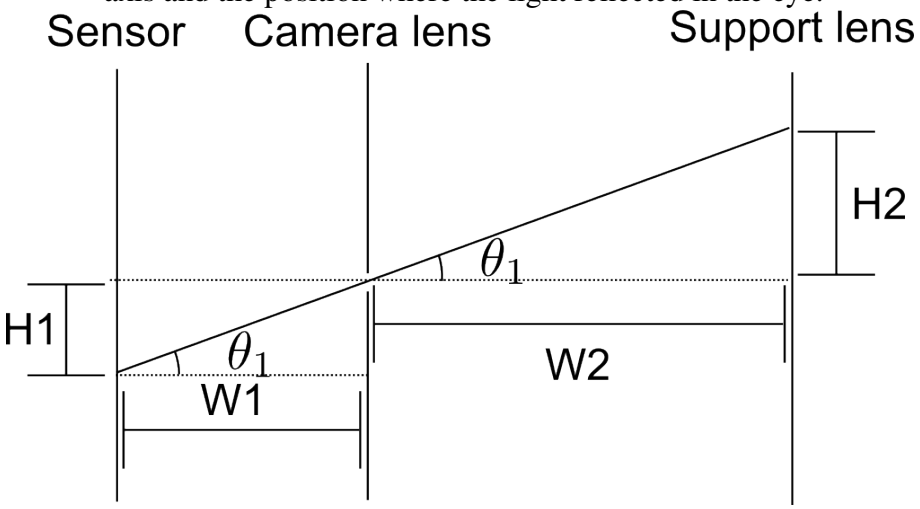

the rings. Next, we present our approach to sample the image and associate the samples with the emitted rings. Finally, we show how to reconstruct the corneal surface using the samples from the previous step.

Figure 4.16: Reconstruction steps.

The captured image from the ring is sampled along meridians, illustrated on the top-left. The reconstruction is performed for each meridian, in point-pair steps (top-right). Iteratively, the algorithm searchs for the next position, based on the approach's restrictions: the two points are connected by a circle arc, preserving the first point normal and respecting the law of reflection in the second point (bottom-right). Finally, the process continues calculating the next point along the meridian.

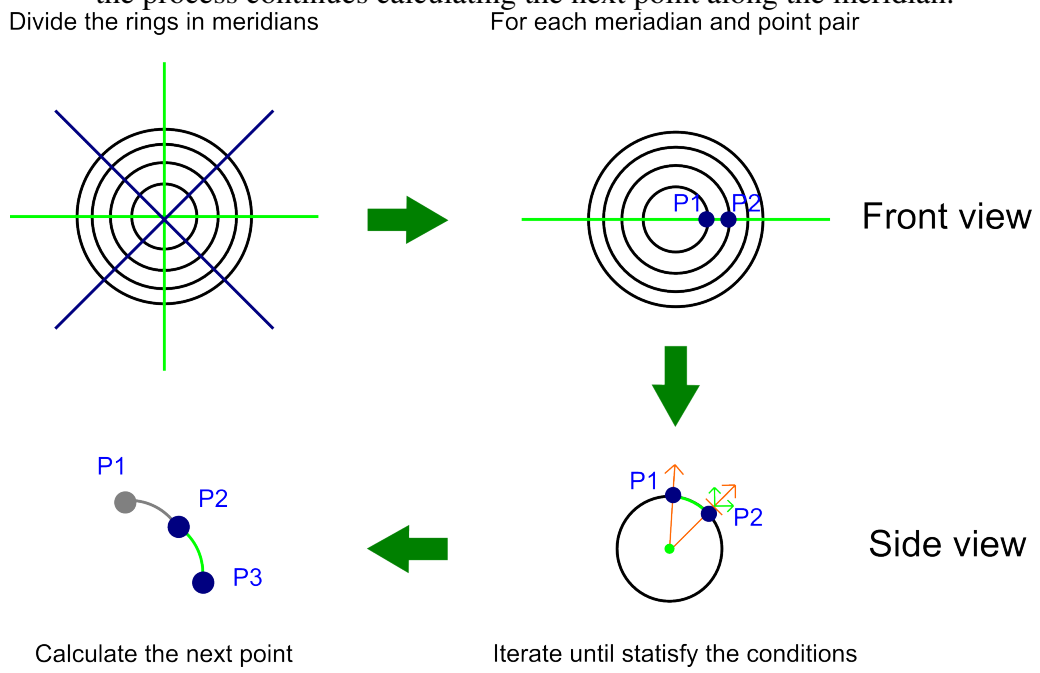

Figure 4.17: Normal calculation.

To calculate the normal for our point we need: the previous point (P1); the previous normal (N1); and the point we are testing (P2) (left). We are approximating the corneal by a circle, a line that passing by N1 will intersect a line that pass by the normal we are calculating, and has the same distance to P1 and P2, respectively. However, there are infinite lines that pass by P2 and intersect the first line (center), and we do not know which is the correct one. If we link P1 and P2 the two lines will be a isosceles triangle, in this case, a line perpendicular to this last line center, will intersect the first line in the third point, hence we can calculate the P2 normal.

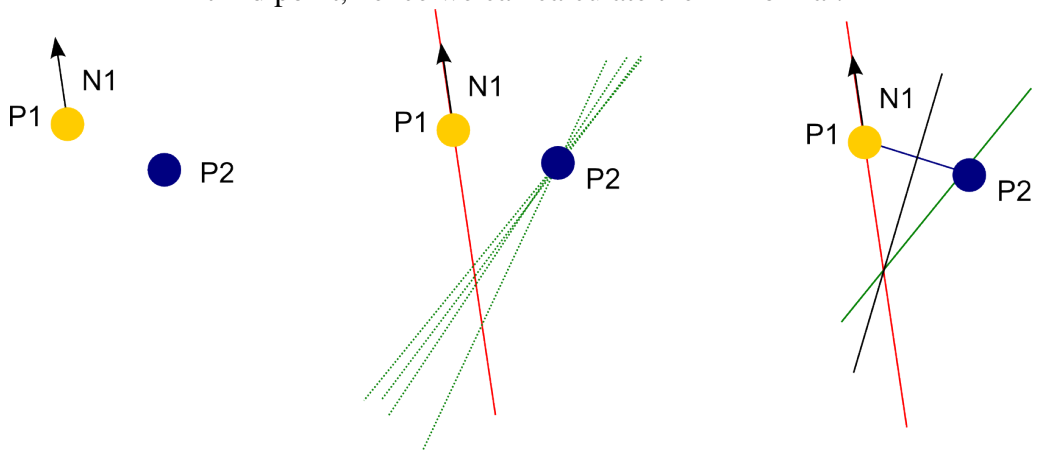

Figure 4.18: Reconstructed surface.

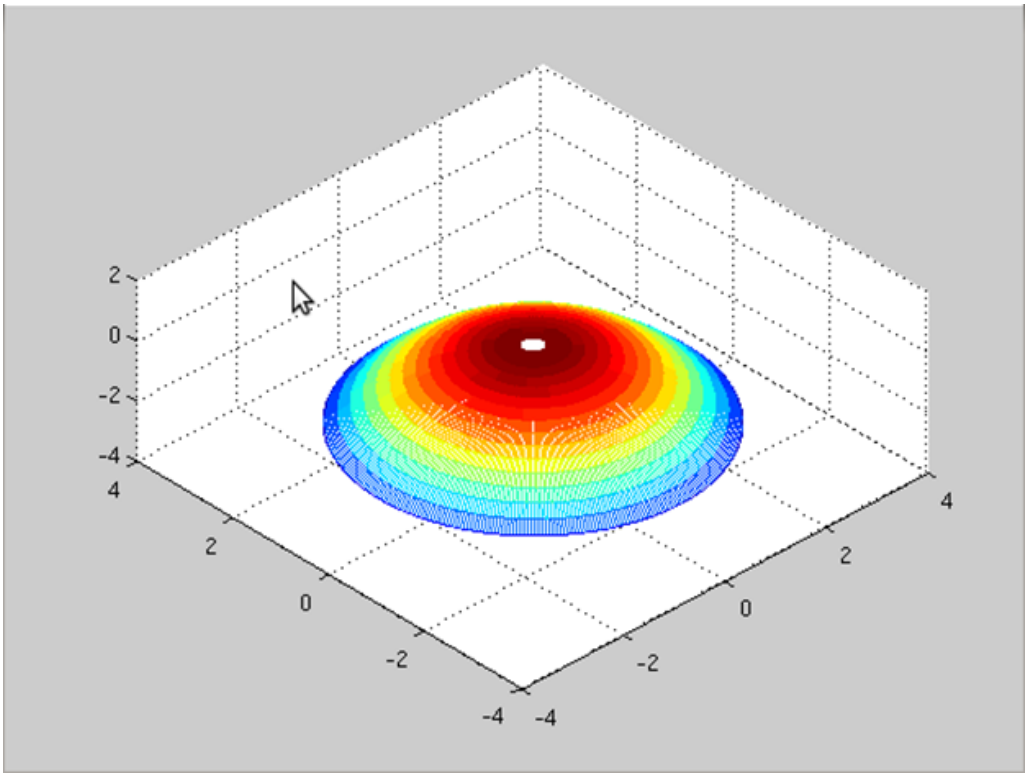

5 EXPERIMENTS AND EVALUATION

In this chapter we evaluate the results produced using our prototype, and procedures to deal with the captured information. We evaluate the results in different ways. First, we present examples of images captured and processed with our system. We also evaluate the ability of our prototype to identify subjects with keratoconus. Finally, we compare the surface produced by our prototype against the ones obtained using a commercial corneal topographer.

5.1 Methods

We analyze the results produced by our prototype in three different ways. First, we present the keratoscopies generated by our prototype. The keratoscopies are the processed images that can be used to perform diagnoses. We compare results obtained for normal eyes and eyes with keratoconus. Keratoconus is a degenerative condition of the eye that causes the cornea to locally assume a conical shape, as opposed to the more natural round shape (Figure 5.1). After that, we analyze the results based on the extracted coefficients for Zernike polynomials. We use the optical meaning associated with keratoconus to correlate the subjects with keratoconus and high coefficients related to high order aberrations. Likewise the correlation between low coefficients with eye without keratoconus. Finally, also using the polynomials, we compare the results produced by our approach with the values obtained using a commercially available Pentacam corneal topographer. We compare the coefficient values and the differences from the reconstructed surfaces obtained with prototype and with the Pentacam.

5.1.1 Zernike Polynomials

Combining the Zernike polynomials obtained from the the captured images, we can reconstruct a surface representing the evaluated eye. Commercial corneal topographers can provide the polynomials coefficients, hence we can use these values for comparison. Besides, each polynomial has an optical meaning, and they are somehow related to high order conditions (i. e., keratoconus). This way, we can perform a screening for keratoconus. The coefficient used for this purpose are those with radial index (n) 3 (see Figure 3.5), that represents trefoil and coma.

5.2 Keratoscopy

The first results that we get are the captured and post processed images, called keratoscopies. We present images produced by different eyes: normals, astigmatics, and with

Figure 5.1: Keratoconus eye.

Image from (COMMONS, 2013b)

keratoconus. To identify the conditions using the images we use the rings that we can see in the images. The rings shape is related to each eye conditions. Normal eyes generate circular rings in the exam, as for instance, in image 5.2.

Astigmatic eyes generate different rings in the image. Since the ring shape depends on the corneal curvature, different curvatures change the rings radii. In astigmatism, there are two main meridians, approximately orthogonal, with minimum and maximum curvature values. The curvature values between these two meridians interpolate these main curvatures. Thus, each meridian has a different curvature and consequently different ring radius, producing elliptical rings. Figure 5.3 shows keratoscopies from subjects with astigmatism. It is not easy to see the elliptical form in the rings. In Figure 5.4 we crop the image shown in Figure 5.3 (top) and put circles (red) and ellipses (blue) close to the rings. Note that the ellipses are closer to the rings than the circle.

Using the same principle, from the astigmatism we can identify keratoconus. In this case, the eye has greater curvature in one side. Hence, the rings from keratoconus are stretched and becomes oval 5.5.

The results presented in this section can be used to screen patients for certain refractive conditions resulting from corneal abnormal shapes. This task can be easier in some cases, such as in the keratoconus cases, or more difficult, such as in the astigmatism cases.

Figure 5.2: Normal eye keratoscopy.

The image shows a keratoscopy from a subject with normal eye. The Placido's rings have approximately circular shapes.

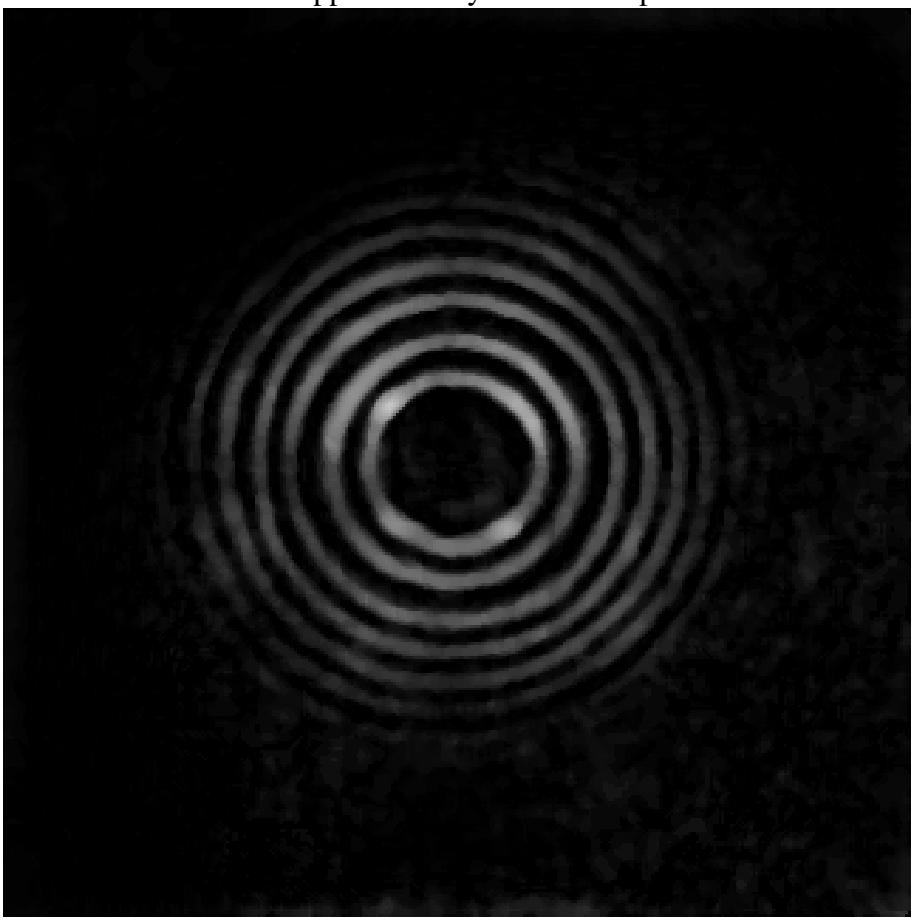

5.3 Keratoconus Identification

After performing the surface reconstruction and fitting Zernike polynomials to it, we have a set of coefficients that describes the corneal surface. In this section, we use these coefficients to determine if the subject has keratoconus or not, or some evidence for this. A keratoconus evidence can be used to help in a pre-trial, and who has evidence is sent to a more expensive exam.

In our study, eleven subjects had their corneal topographies acquired with our topographer. The subjects include 9 males (ages from 22 to 47) and 2 females (ages from 22 to 25). Our tests were not double blind, because we needed subjects with keratoconus. Thus, we had to ask people if they have this condition. Table 5.1 shows the obtained Zernike coefficients associated with the high-order terms related to keratoconus (trefoil and coma). The tested subjects already knew if they have keratoconus or not from previous examination.

First, we show the values from the coefficient associated with high order aberrations from our trials. Table 5.1 shows the values from coma and trefoil computed for each subject using our prototype. From the meaning of the Zernike coefficients we know that the existence of one or more coefficients with higher magnitude suggests a high probability of the subject having keratoconus. Looking at these data, we can see values with high differences in comparison with the others. Subject 3 has a coma coefficient of 18.5

Figure 5.3: Astigmatism cases

Eyes with astigmatism change the Placido's rings shape, the rings become closer to ellipses than circles.

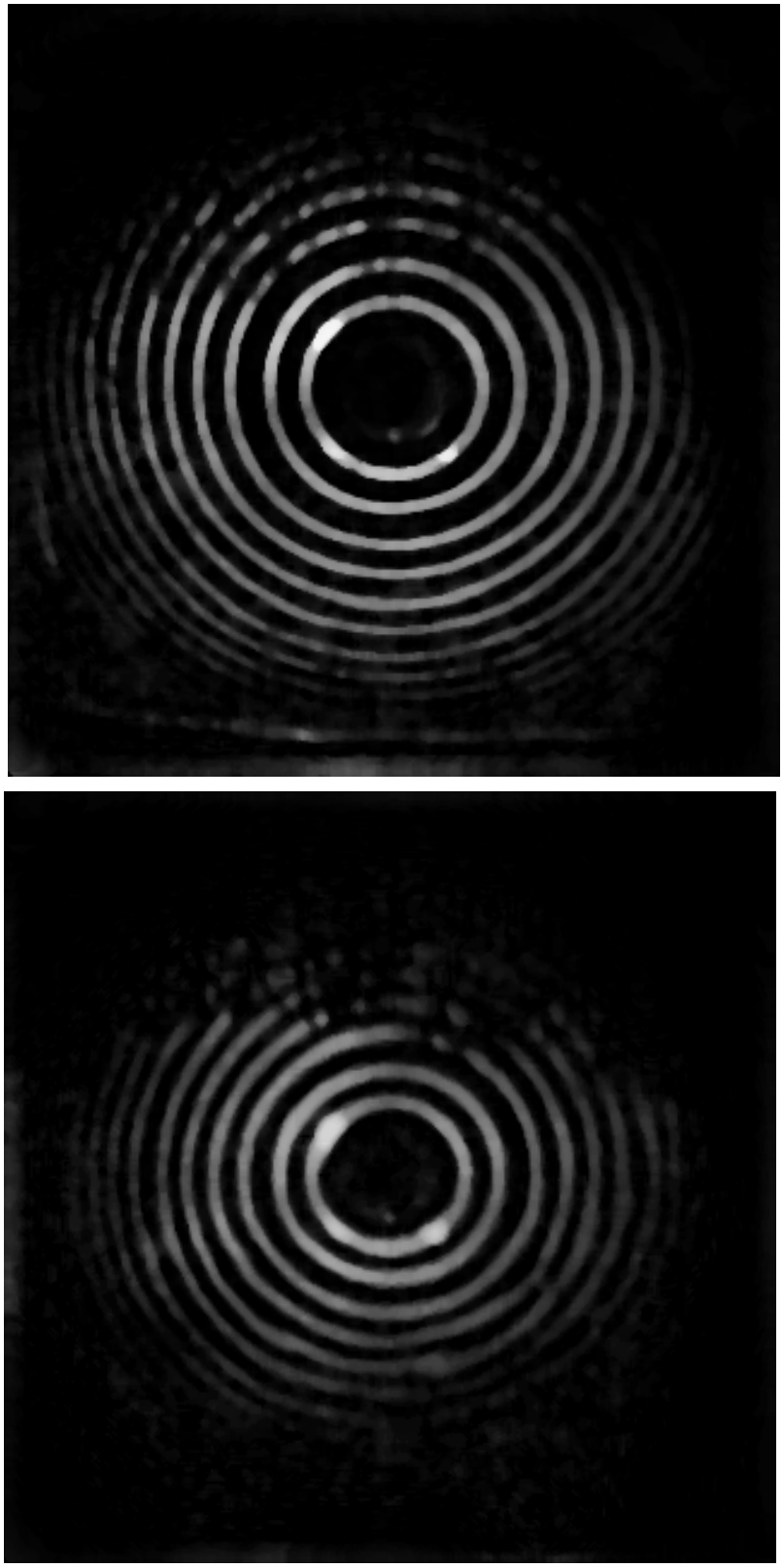

Figure 5.4: Astigmatism case zoom

To help to note the more elliptical shape in the astigmatics cases, we draw circles and ellipses in a zoom from one astigmatic keratoscopy. The circles (red) were adjusted by the rings height. While the ellipses (blue) were adjusted using the rings height and width. Note the differences in the width between the circles and the ellipses.

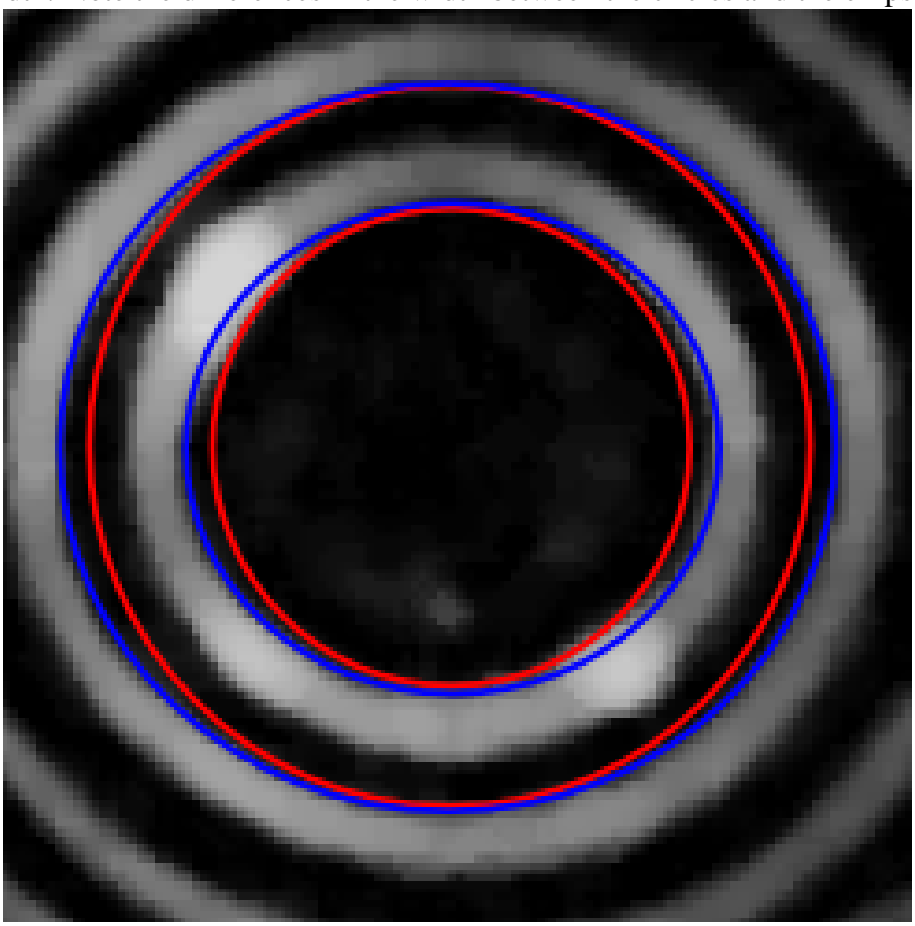

micrometers, which suggests a high probability of having keratoconus. Another subject likely to have keratoconus is subject 8, with coma values of 11.1 and 5.3 micrometers. Subject 4 is next, with a coma of 5.6 micrometers and a trefoil of -4.8 micrometers (although not as high as the previous two subjects, these values still seem to be relevant). Subjects 6, 7 and 9 also have substantial values for these coefficients.

Only observing the data from our tests we guess the most likely subjects to have keratoconus (Table 5.2). According to corneal topography performed using a commercial equipment (they performed the tests with their doctors), the first three subjects in Table 5.2 indeed do have keratoconus. Thus, high-magnitude values associated with high-order aberration coefficients are indeed good predictors of the occurrence of keratoconus. We do not have a threshold to define when a subject has keratoconus.

5.4 Pentacam Comparsion

To validate our results compared the values obtained with our prototype against the ones obtained with a commercial corneal topographer (Pentacam). This device is used by doctors to perform diagnostics, so we use it as ground truth. Four subjects had corneal topography ofr both eyes performed with the Pentacam. From these, one subject has

Table 5.1: High order coefficient from keratoconus identification trials.

The table shows the coefficients from the Zernike polynomials associated with high order aberrations (i. e. keratoconus).

	Trefoil (3,-3)	Coma (3,-1)	Coma (3, 1)	Trefoil (3,3)
Subject 1	0.867 μm	-0.1081 μm	1.5991 μm	-1.5575 μm
Subject 2	-0.4322 μm	1.5724 μm	1.7477 μm	-0.1758 μm
Subject 3	1.2282 μm	-1.188 μm	18.5596 μm	-5.6078 μm
Subject 4	-4.8245 μm	0.255 μm	5.6711 μm	-0.3516 μm
Subject 5	-0.0942 μm	-0.7877 μm	1.1189 μm	0.2437 μm
Subject 6	-0.1445 μm	-1.3778 μm	2.7242 μm	-1.3965 μm
Subject 7	-0.5572 μm	0.5049 μm	3.2334 μm	0.3261 μm
Subject 8	2.3114 μm	5.3911 μm	11.1504 μm	-2.994 μm
Subject 9	0.2369 μm	-0.8915 μm	-2.9229 μm	0.3136 μm
Subject 10	-0.4358 μm	0.4473 μm	-1.2392 μm	0.522 μm
Subject 11	-0.4233 μm	0.1412 μm	-1.4098 μm	-0.6509 μm

Table 5.2: Subjects we estimate to be more likely to have keratoconus, based on high values of the Zernike coefficients associated with such condition.

The table was sorted by them sum of the absolute coefficients values.

	Trefoil	Coma	Coma	Trefoil	Has keratoconus?
Subject 3	1.2282 μm	-1.188 μm	18.5596 μm	-5.6078 μm	yes
Subject 8	2.3114 μm	5.3911 μm	11.1504 μm	-2.994 μm	yes
Subject 4	-4.8245 μm	0.255 μm	5.6711 μm	-0.3516 μm	yes
Subject 6	-0.1445 μm	-1.3778 μm	2.7242 μm	-1.3965 μm	no
Subject 7	-0.5572 μm	0.5049 μm	3.2334 μm	0.3261 μm	no
Subject 9	0.2369 μm	-0.8915 μm	-2.9229 μm	0.3136 μm	no

Figure 5.5: Keratoscopy of a subject with keratoconus.

The keratoconus eye has an irregular shape, one side is deformed and less curved. This is reflected in the keratoscopies. Note the oval shape from the rings.

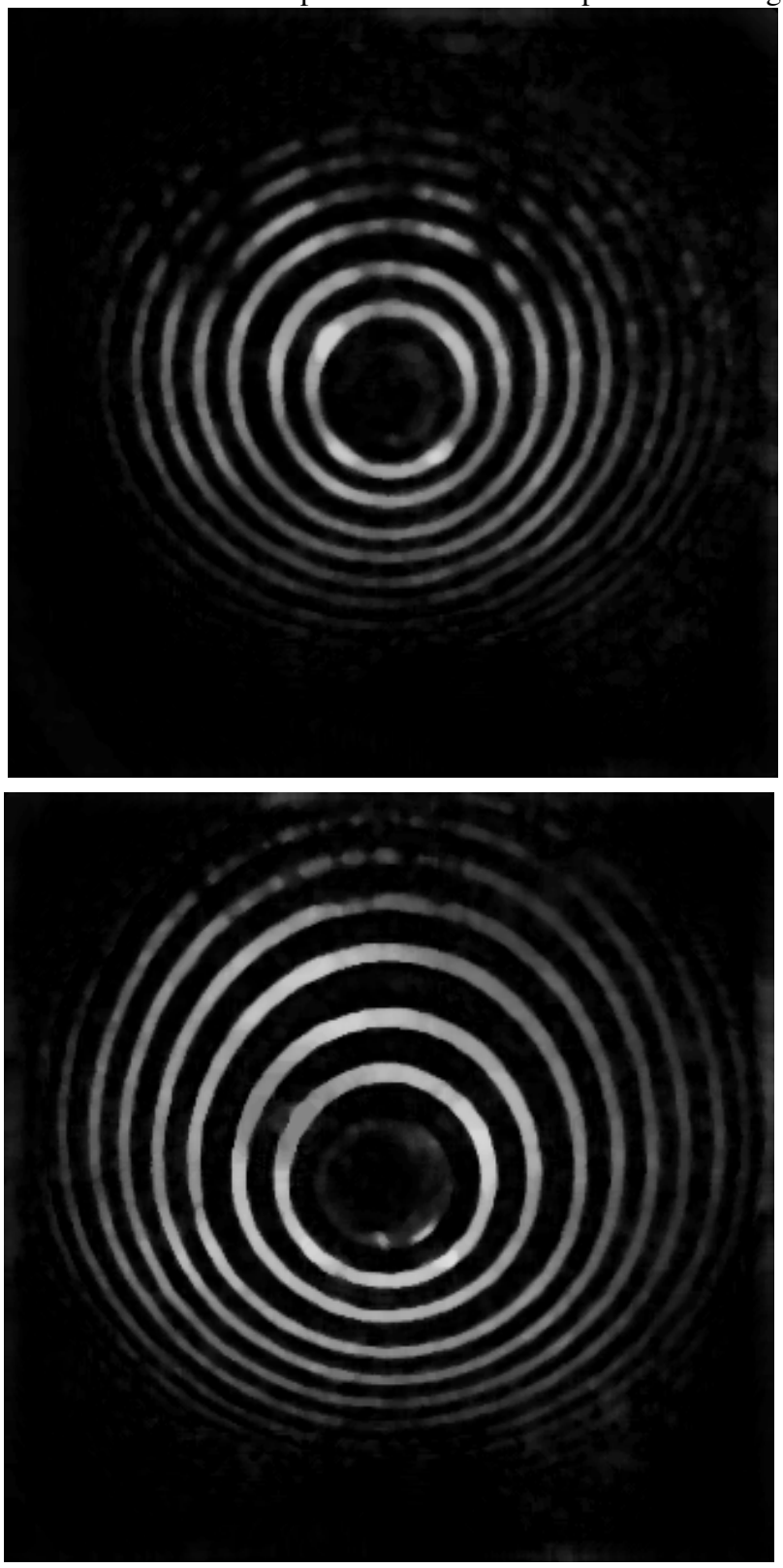

keratoconus on two eyes. Since we have the exams we need to compare the values.

Table 5.3: Zernike coefficient comparison example.

This table shows raw Zernike coefficient comparison between the Pentacam and our prototype. Directly comparing the coefficient values it is hard to predict the differences between the surfaces estimated by the two systems, as the surfaces are linear combinations of various basis surfaces, which may compensate each other.

Index		Eye 1		Eye 2	
n	m	Pentacam	Our	Pentacam	Our
0	0	301.355 μm	272.5087 μm	323.587 μm	339.9306 μm
1	1	-1.072 μm	6.6963 μm	18.231 μm	6.1913 μm
1	-1	2.035 μm	-8.3894 μm	-40.818 μm	-38.9654 μm
2	2	-2.197 μm	0.0032 μm	-7.566 μm	-7.3073 μm
2	0	175.873 μm	169.7289 μm	187.907 μm	211.5259 μm
2	-2	0.917 μm	1.4468 μm	5.435 μm	-2.368 μm
3	3	0.128 μm	-0.4358 μm	-0.626 μm	-0.3581 μm
3	1	-0.232 μm	0.4473 μm	4.396 μm	0.451 μm
3	-1	0.536 μm	-1.2392 μm	-9.436 μm	-13.0718 μm
3	-3	0.008 μm	0.522 μm	-0.207 μm	-0.0827 μm
4	4	-0.171 μm	-0.5408 μm	-0.196 μm	-0.4188 μm
4	2	-0.124 μm	0.4179 μm	-1.316 μm	-2.5785 μm
4	0	1.516 μm	2.7072 μm	0.877 μm	5.2661 μm
4	-2	0.051 μm	-0.1994 μm	-0.988 μm	-0.2147 μm
4	-4	-0.043 μm	0.3028 μm	-0.339 μm	0.4535 μm

The Pentacam provides a list with the Zernike polynomials coefficients. As our prototype also provides these coefficient as a result, we compare the values using the polynomials. The first idea is to compare the raw coefficients, but it is difficult to quantify the differences. For instance, Table 5.3 shows the coefficient values from the Pentacam and from our prototype for two eyes. The measurements are in micrometers, hence the difference is also in micrometer scale. Note that values have a similar profile, the values magnitudes are close. From these values it is hard to figure out the difference between the actual topographic surfaces.

To better compare these results, we use other approach to analyze the data. We evaluate the polynomials using the coefficient from the two devices using the set of spherical coordinates (θ, ϕ) values. Hence, we know the difference between the two surfaces at each pair of spherical-coordinate values. Using samples from all over the surface, we get a good estimate about the general surface differences.

To analyze the information about the surface differences, first we plot histograms from the differences. We use 5,760 samples from the surfaces, distributed over 16 concentric circles centered at the center of the pupil (Figure 5.6). Looking at the histograms, Figure 5.7, one observes that the majority of difference values are under 0.02 millimeters, and the biggest differences are around 0.14 millimeters, with a very-low frequency.

From these data, we also calculate the mean and standard deviation. The Table 5.4 shows the values from the eight examined eyes. Both mean and standard deviation values are around 10^{-2} millimeters. To give an idea about the representativeness of these values, we compare the values with the mean anterior corneal radius, which has a value of 7.8 millimeters (SCHWIEGERLING, 2004). We use these values to calculate how much the

Figure 5.6: Sampled points.

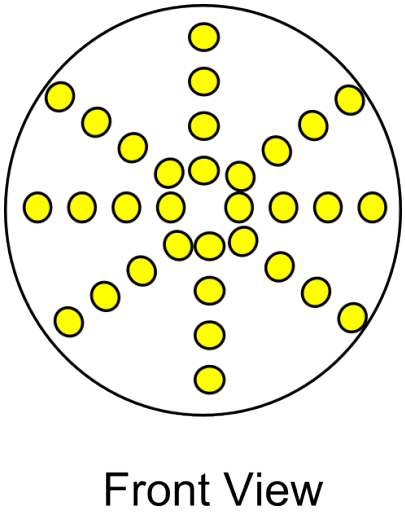

Table 5.4: Mean and standard deviation from the surfaces differences.

We compare the values we get from the Zernike polynomial evaluation using the same parameters for each sample and the coefficients generated by our prototype and by Pentacam.

	Mean	Standard deviation
Eye 1	0.0401 mm	0.0225 mm
Eye 2	0.0350 mm	0.0202 mm
Eye 3	0.0211 mm	0.0218 mm
Eye 4	0.0280 mm	0.0296 mm
Eye 5	0.0224 mm	0.0144 mm
Eye 6	0.0254 mm	0.0134 mm
Eye 7	0.0202 mm	0.0209 mm
Eye 8	0.0186 mm	0.0089 mm

differences represent. Based on the higher value in the Table 5.4, the difference in the corneal radius corresponds to 0.51% of the typical value.

We also evaluate the differences over various concentric circles (radii), in relation to eye center. Figure 5.8 shows a graphic with the mean differences for each sampled radius. We can see an increasing trend in the graphics. This can be explained because of the reconstruction algorithm uses the value from previous iteration to calculate the next, where differences are incremented in each iteration. Note that the corneal central region has a smaller mean error difference than the mean of the entire corneal surface. We can see in the graph that the mean difference in the first millimeters is below 0.02 millimeters, equivalent to 0.25% from the corneal mean radius.

Analyzing the data we see that our prototype produces a surface that has differences in the order of 10^{-2} millimeters. The bigger mean difference is about 0.51% of the mean anterior corneal radius (the size of a normal eye). In the central region (about 1 millimeter from the eye center), the difference is equivalent to 0.25% of the mean anterior corneal radius, or 0.02 millimeters. We observe that the majority of the differences are under 0.02 millimeters.

5.5 Summary

In this chapter we analyzed the result obtained with the proposed prototype in three ways: acquired keratoscopies, the Zernike coefficient values, and finally, we compared our results with a commercial topographer, the Pentacam.

Using the keratoscopies we are able to see the distortions in the pattern from different conditions. Analyzing the coefficients values that we get and the previous information about the coefficient meaning, we identify subjects that are likely to have keratoconus, and the ones we classify as most likely have the condition. Finally, we compared the surfaces generated by our prototype and by the Pentacam, the mean differences between them are around 0.02 millimeters, which corresponds to 0.51% of the mean anterior corneal radius.

Figure 5.7: Histograms of surface differences.

Histograms for each eye with difference magnitudes, in millimeters, from the surfaces produced by our prototype and by the Pentacam. The three first rows are from eye without high order aberrations and the last row is from eyes with keratoconus.

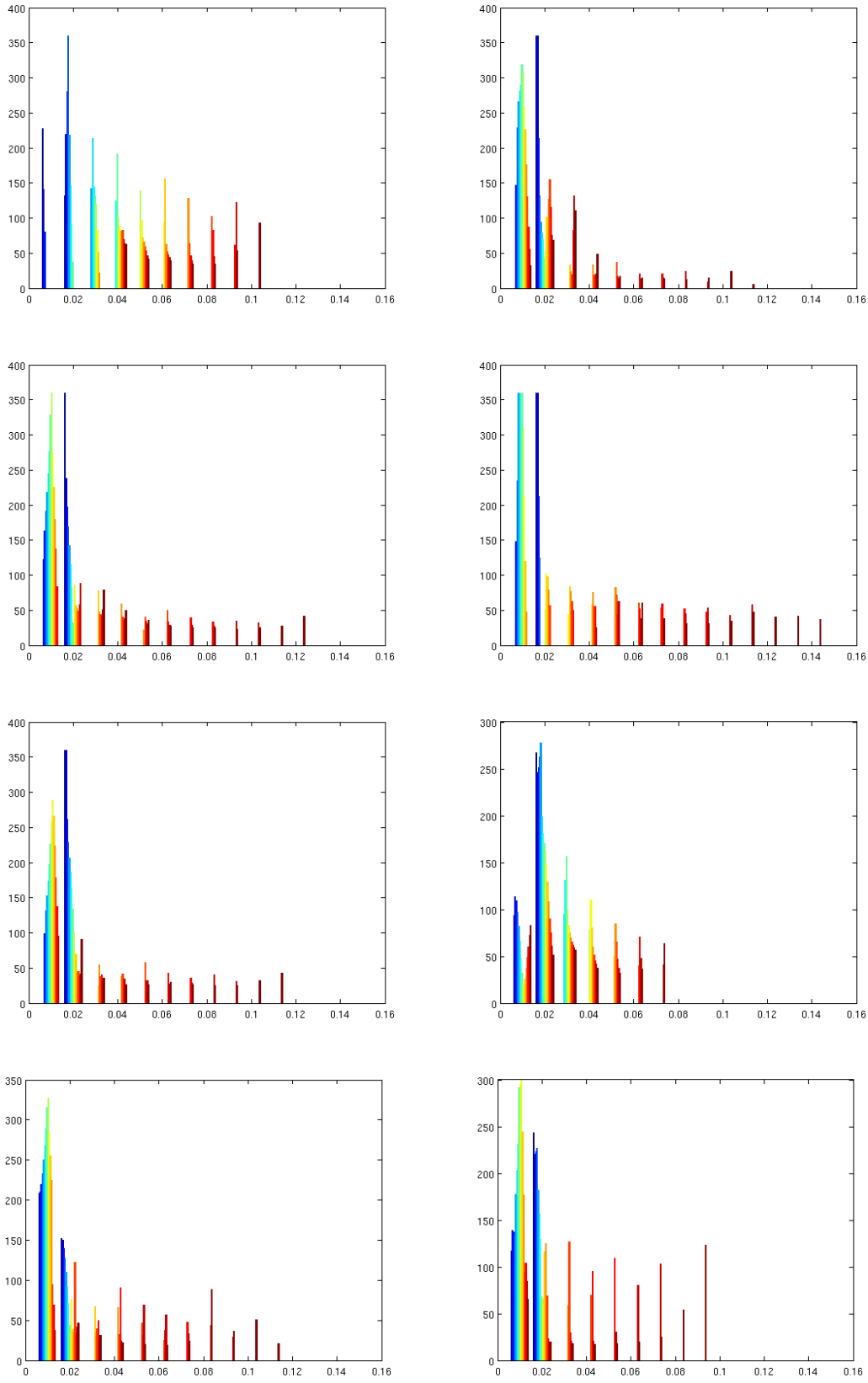

Figure 5.8: Mean differences by radius.

The figure shows a graphic from the mean surface differences (vertically) by the sample radius (horizontally), with respect to eye center. The values are in millimeters.

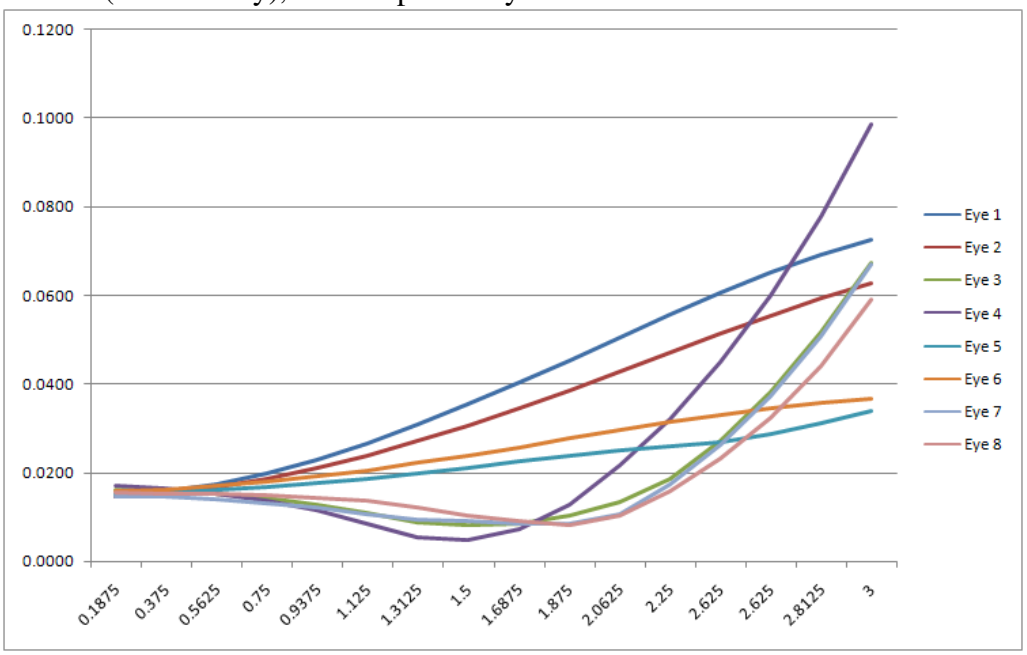

6 CONCLUSIONS

We have introduced a corneal topographer with low cost and high mobility, that we call an accessible topographer. Based on the Placido's disk fundamentals, we built a portable and inexpensive topographer.

The corneal shape, measured with corneal topographers, is important to the image formation. This way, corneal topography is used in several applications in ophthalmology, such as keratoconus detection, contact lens fitting; and refractive pre- and post-operatory procedures.

Our prototype uses a cell-phone to capture images. The images capture the reflected Placido's disks emitted by our prototype. The deformations in these patterns define the corneal surface shape.

After capturing the reflected pattern, with their deformations, we transfer the images to a personal computer and use a sequence of image processing algorithms to improve image quality and extract the rings. Next, the extracted rings are associated with the emitted ones. In many cases, a simple approach to make these operation can do wrong associations, we developed a method that identifies and fixes missing portions of the projections of the circular patterns.

Next, the ring information is sampled and used as input to the reconstructed algorithm. The algorithm searches iteratively for a surface that best fits the samples. After that, we fit the obtained surface using Zernike polynomials to decompose it in components with specific meaning.

Given the obtained Zernike coefficients, we evaluate the results produced in this work. First, we evaluate the captured and enhanced images, called keratoscopies, for corneas with different conditions. Next, we use the polynomials and the previous knowledge about their optical meanings to rank the eyes according to their likelihood of not having keratoconus. In our experiments, the top three ranked eyes indeed had keratoconus.

We have compared the results obtained with our prototype against the ones provided by the Pentacam, a commercially available corneal topographer. For this, we computed the differences between the reconstructed surfaces by both devices. We verify that the mean difference is about 0.02 millimeters, which represent 0.5% of the mean anterior corneal radius.

We conclude that a device able to perform corneal measurements with low cost is possible, as we have demonstrated. Accessible devices can be very useful for patient screening, where people with potential conditions could be sent to specific treatment.

Our current corneal topographer prototype has some limitations. First, the image-processing pipeline is performed on a personal computer, requiring the download of the images captured with cell phone camera. The clip-on device for projecting the pattern contains 36 LEDs and requires an electrical outlet to provide power. For stability, image

acquisition is performed by placing the prototype on a flat horizontal surface. Due to blurring caused by defocusing or patients movement, one may need to capture a few images (typically up to 3) before acquiring a proper image for processing.

6.1 Future Work

We see some direct improvements to our prototype: the topographer could be smaller than it is, becoming even more portable; moreover, all the implementations may be ported to the cell-phone, also helping the portability. The system may generate standard reports that doctors use currently in their offices. The prototype could be ported to be used with other cell-phone models to facilitate the use for different people. Finally, more extensive tests should be performed to verify the repeatability of the device.

REFERENCES

ACHARYA, T.; RAY, A. K. **Image Processing Principles and Applications**. [S.l.]: John Wiley & Sons, 2005.

AGARWAL, A.; AGARWAL, A.; JACOB, S. **Corneal Topography**. [S.l.]: Anshan, 2009.

ALKHALDI, W. et al. Enhancing the Standard Operating Range of a Placido Disk Videokeratoscope for Corneal Surface Estimation. **Biomedical Engineering, IEEE Transactions on**, [S.l.], v.56, n.3, p.800 –809, march 2009.

CANEIRO, D. A.; ISKANDER, D. R.; COLLINS, M. J. Estimating Corneal Surface Topography in Videokeratoscopy in the Presence of Strong Signal Interference. **IEEE Trans. Biomed. Eng.**, [S.l.], v.55, p.2381–2387, 2008.

CANNY, J. A Computational Approach to Edge Detection. **IEEE Trans. Pattern Anal. Mach. Intell.**, Washington, DC, USA, v.8, n.6, p.679–698, June 1986.

CARLETON, O. **Bon Optic Eye Top Corneal Topographer**. `http://www.carletonltd.com/products/corneal/topography/bon-optic-eye-top-corneal-topographer-0`. [Online; accessed 10-April-2013].

CARLETON, O. **Bon Optic Eye Top Corneal Topographer**. `http://www.carletonltd.com/products/corneal/topography/bon-optic-eye-top-2-h-corneal-topographer`. [Online; accessed 10-April-2013].

COMMONS, W. **Zernike Polynomails**. `http://commons.wikimedia.org/wiki/File:ZernikePolynome6.svg`. [Online; accessed 10-April-2013].

COMMONS, W. **Keratoconus eye**. `http://en.wikipedia.org/wiki/File:Keratoconus_eye.jpg`. [Online; accessed 10-April-2013].

CSO, O. **Focus portable corneal Topographer**. `http://www.csophthalmic.com/english/topographers/focus/index.html`. [Online; accessed 10-April-2013].

CSO, O. **CM02/CM-P02 Corneal Topographer**. `http://www.csophthalmic.com/english/topographers/cm02/index.html`. [Online; accessed 10-April-2013].

CSO, O. **CSO Eye Top2005 LITE FOCUS corneal Topographer**. http://www.csophthalmic.com/english/topographers/eyetoplite/index.html. [Online; accessed 10-April-2013].

DOSS, J. D. et al. Method for calculation of corneal profile and power distribution. **Arch Ophthalmology**, [S.l.], v.99, p.1261–1265, 1981.

EYESYS, V. **EyeSys System 3000**. http://www.eyesys.com/products_system3000.asp. [Online; accessed 09-April-2013].

EYESYS, V. **EyeSys V**. http://www.eyesys.com/products_vista.asp. [Online; accessed 09-April-2013].

HALSTEAD, M. A. et al. Reconstructing curved surfaces from specular reflection patterns using spline surface fitting of normals. In: COMPUTER GRAPHICS AND INTERACTIVE TECHNIQUES, 23., 1996, New York, NY, USA. **Proceedings...** ACM, 1996. p.335–342. (SIGGRAPH '96).

ITALIA, C. **Topograpfo**. http://www.csoitalia.it/TOPOGRAFO_2.html. [Online; accessed 12-April-2013].

JONGSMA, F.; BRABANDER, J. de; HENDRIKSE, F. Review and Classification of Corneal Topographers. **Lasers in Medical Science**, [S.l.], v.14, p.2–19, 1999. 10.1007/s101030050015.

KLEIN, S. A. A Corneal Topography Algorithm that Produces Continuous Curvature. **Optometry and Vision Science**, [S.l.], v.69, n.69, p.829–834, 1992.

KLEIN, S. A. Corneal Topography Reconstruction Algorithm that Avoids the Skew Ray Ambiguity and the Skew Ray Error. **Optometry and Vision Science**, [S.l.], v.74, n.11, p.945–962, 1997.

KLEIN, S. A. Corneal Topography: a review, new ansi standards and problems to solve. **Vision Science and its Applications**, [S.l.], p.NW8, 2000.

LIM, J. S. **Two-Dimensional Signal and Image Processing**. Englewood Cliffs, NJ: Prentice-Hall, 1990.

MEDMONT. **E300 Corneal Topographer**. http://www.medmont.com.au/products/e300-corneal-topographer.aspx. [Online; accessed 12-April-2013].

MERKLINGER, H. M. **Focusing The View Camera**. [S.l.]: Seaboard Printing Limited, 1996.

NAKAGAWA, T. et al. Higher-Order Aberrations Due to the Posterior Corneal Surface in Patients with Keratoconus. **Invest. Ophthalmol. Vis. Sci.**, [S.l.], v.50, n.6, p.2660–2665, Jun 2009.

NOKIA. **Nokia N900 - Specifications - Nokia - UK**. http://www.nokia.com/gb-en/phones/phone/n900/specifications/. [Online; accessed 10-April-2013].

NOLL, R. J. Zernike polynomials and atmospheric turbulence. **J. Opt. Soc. Am.**, [S.l.], v.66, n.3, p.207–211, Mar 1976.

OCULUS. **The measurement principle**. http://www.pentacam.com/sites/messprinzip.php. [Online; accessed 09-April-2013].

OPTIKON. **Keratron**. http://www.optikon.com/en/keratron.asp. [Online; accessed 11-April-2013].

OPTIKON. **Keratron Scout**. http://www.optikon.com/en/keratronscout.asp. [Online; accessed 11-April-2013].

OPTIKON. **Keratron Piccolo**. http://www.optikon.com/en/keratronpiccolo.asp. [Online; accessed 11-April-2013].

OPTIKON. **Keratron Onda**. http://www.optikon.com/en/keratrononda.asp. [Online; accessed 11-April-2013].

PAMPLONA, V. F. et al. NETRA: interactive display for estimating refractive errors and focal range. **ACM Trans. Graph.**, [S.l.], v.29, n.4, 2010.

PAMPLONA, V. F. et al. CATRA: interactive measuring and modeling of cataracts. **ACM Trans. Graph.**, New York, NY, USA, v.30, p.47:1–47:8, August 2011.

PLACIDO, A. Novo instrumento de esploraÃ§Ã£o da cornea. **Periodico d'Opthalmologica Practico**, [S.l.], v.5, p.27–30, 1880.

RAND, R. H.; HOWLAND, H. C.; APPLEGATE, R. A. Mathematical Model of a Placido Disk Keratometer and Its Implications for Recovery of Corneal Topography. **Optometry and Vision Science**, [S.l.], v.74, p.926–930, 1997.

SCHWIEGERLING, J. **Field guide to visual and ophthalmic optics**. [S.l.]: International Soceity for Optical Engineering, 2004.

SCHWIEGERLING, J.; GREIVENKAMP, J. Using Corneal Height Maps And Polynomial Decomposition to Determine Corneal Aberrations. **Optometry and Vision Science**, [S.l.], v.74, p.906–916, 1997.

SIGHT, L. http://www.lase.com/rsastramax.htm. [Online; accessed 10-April-2013].

TOMEY. **TMS-5 | Tomey**. http://www.tomey.com/Products/Topography/TMS-5.html. [Online; accessed 12-April-2013].

VILA, I. et al. A robust method for extracting and labelling mires in keratographic images. In: ENGINEERING IN MEDICINE AND BIOLOGY SOCIETY, 1995., IEEE 17TH ANNUAL CONFERENCE, 1995. **...** [S.l.: s.n.], 1995. v.2, p.1431 –1432 vol.2.

ZHOU, H.; WU, J.; ZHANG, J. **Digital Image Processing - Part II**. [S.l.]: Ventus Publisher ApS, 2010.

ZIEMER, O. **Ziemer Opthalmic Systems AG**: galilei g2. http://www.ziemergroup.com/products/galilei.html. [Online; accessed 11-April-2013].

APPENDIX A UMA ABORDAGEM ACESSÍVEL PARA TOPOGRAFIA DA CÓRNEA

Resumo da Dissertação em Português

A evolução tecnologica faz com que a maioria dos dispositivos se torne mais acessível. Porém, isto não é uma realidade em todas as aplicações. Topografia da córnea é uma área que não tira muita vantagem dessa evolução. Na oftalmologia, ela tem aplicações no diagnostico de ceratocone, pré e pos-procedimentos de cirurgias refrativas, e ajuste de lentes de contato. O primeiro método para examinar a topografia da córnea é o disco de Plácido (PLACIDO, 1880). Ele é basicamente um disco que tem círculos concêntricos que se alternam entre pretos e brancos, com um furo no centro. O observador olha no olho do paciente pelo orifício é o observa as deformações definidas pela superfície da córnea. Este método evoluiu para abordagens automatizadas onde o olho do observador é substituído por uma câmera (ver Figura A.1) e técnicas de processamento de imagens são utilizadas para reconstruir uma mapa acurado da córnea. Existem três métodos principais para reconstrução da córnea, que são baseados em: reflexão especular usando o disco de Plácido; triangulação usando luzes estruturadas; e interferometria (KLEIN, 2000). Abordagens inspiradas no disco de Plácido usam um padrão com anéis circulares que são refletidos na superfície da córnea e capturados por um sensor. Métodos de triangulação usam luz estruturada (um tabuleiro de xadrez, por exemplo), refletida difusamente na córnea e também capturada por uma câmera. Como as córneas produzem reflexões especulares, algumas abordagens são utilizadas para produzir reflexões especulares. Dentre estas podemos incluir o uso de luz ultravioleta na fonte de luz, e o uso de fluoresceína de sódio no olho com luz azul (SCHWIEGERLING, 2004). Uma diferença básica entre os dois metódos é a forma que são feitas as medidias: métodos baseados em reflexão especular medem inclinação; abordagens baseadas em triangulação medem alturas. Por fim, abordagens baseadas em interferometria usam um padrão de interferencia de uma fonte de luz de refletidas na olho e em uma forma de referência para medias a forma da córnea. Métodos baseados em interferometria são os mais acurados, mas são muitos sensíveis. Devido as técnicas de suporte necessários para a triangulação e a alta complexidade da interferometria, um dispositivo de baixo custo é mais facilmente alcançavel utilizando uma abordagem inspirada no disco de Plácido. Para construir um topografo são necessários: uma fonte para o padrão (i.e. circulos concêntricos); um dispositivo para a captura da superfície com o padrão refletido; e um dispositivo para processar o algoritmo de reconstrução. Estes são requerimentos relativamente simple de atender, mas um topografo acessível ainda não foi construido. Nosso objetivo é confirmar a intuição e construir este

Figura A.1: Placido's disk based on corneal condition diagnosis.

O topografo de Plácido foi concebido para uso manual (a), onde um observador olha o padrão refletido por um buraco no disco. Topografos modernos baseados no disco de Plácido substituem o observador por uma câmera (b). As images capturadas são processadas para que a superfície da córnea seja estimada.

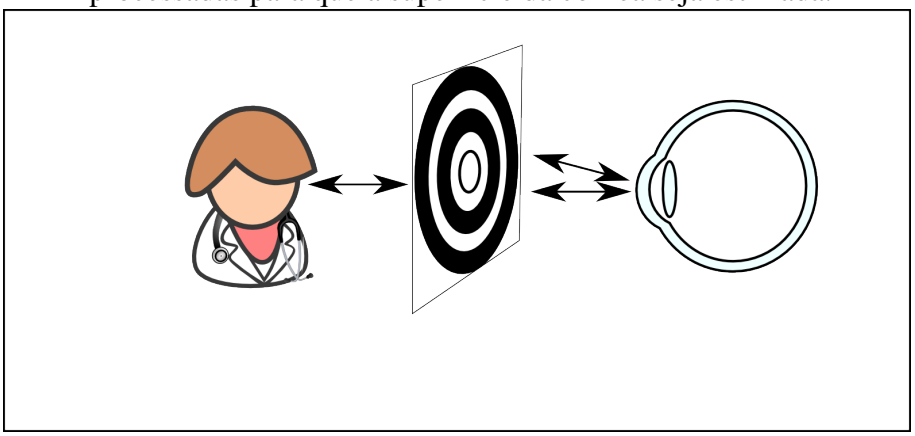

(a) Medição manual com o disco de Plácido

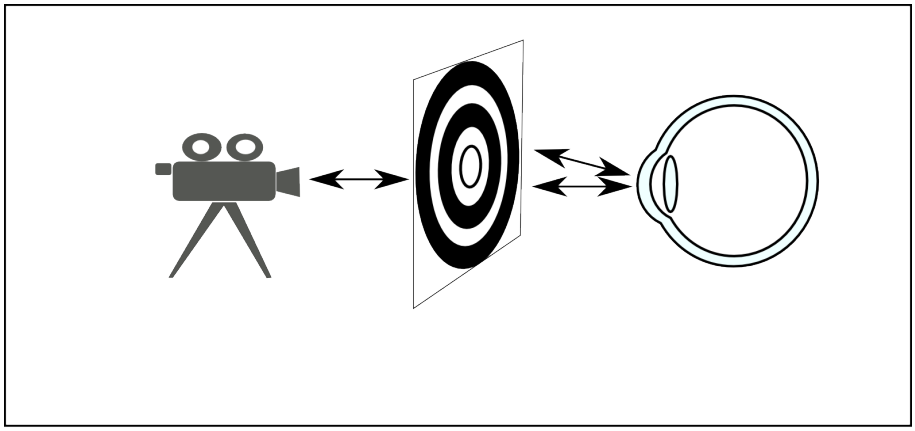

(b) Sistemas modernos baseados no disco de Plácido

topografo. Também é nosso objetivo descobrir a acuracia deste topografo em comparação com dispositivos comerciais e suas possivéis aplicações.

A.1 Dispositivo desenvolvido

Para fazer a reconstrução da superfície da córnea precisamos de um dispositivo para capturar os padrões refletidos na córnea. Assim nós desenvolvemos um baseado em um celular com câmera para a captura da imagem da córnea. Nosso emissor foi desenvolvido de forma a capturar uma imagem da córnea com a câmera no centro dos anéis. Além disso, procuramos desenvolver um dispositivo simples de construir. A seguir, a implementação do dispositivo é discutida.

Considerando que dispositivos móveis tem grande disponibilidade, elessão uma boa opção para o nosso protótipo, desta forma usaremos um celular como o nosso dispositivo de captura. Com isso, nós precisamos incluir as partes que faltam para que consigamos uma imagem dos padrões refletidos na córnea. Para isso, nós precisamos de uma fonte de luz para o nosso padrão, e uma forma de emitir os padrões desejados.

Figura A.2: Modelo conceitual do protótipo.

O nosso dispositivo é composto por três camadas: a primeira fornece iluminação para a projeção dos padrões; a segunda é utilizada para melhorar a difusão da luz emitida, e para colocar a lente utilizada para melhorar a qualidade da imagem capturada; a última é usada com camada de atenuação, está camada é responsável por definir a forma do padrão emitido. Uma visão perspectiva do protótipo proposto é mostrada em (a), e uma visão lateral em (b).

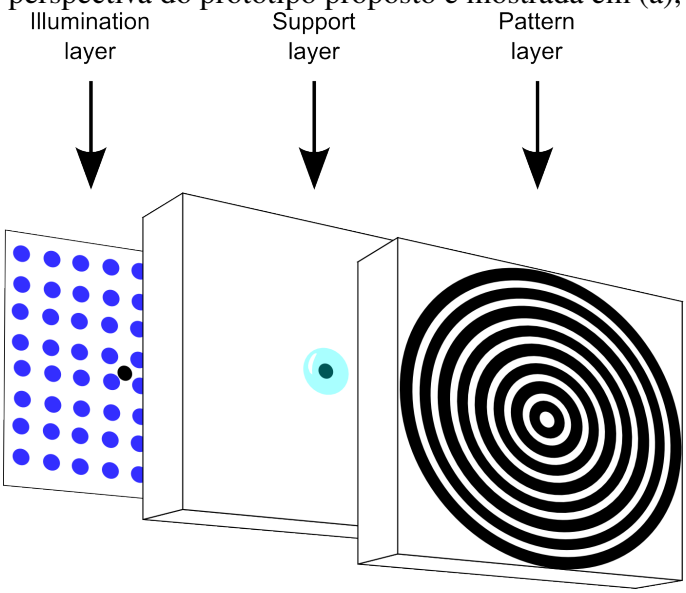

(a) Modelo conceitual do protótipo

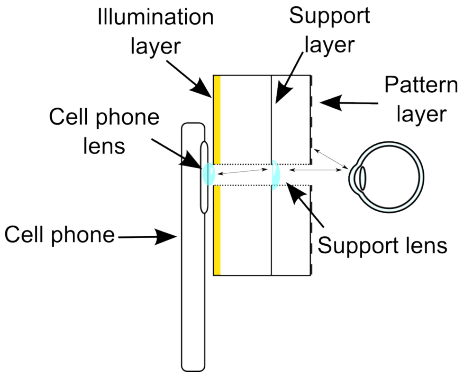

(b) Visão lateral do protótipo

Para fazer isso, nós desenvolvemos um dispositivo com várias camadas. A primeira fornece a iluminação; a segunda é usado como camada de suporte, ajudando com a imagem capturada usando uma lente e também na difusão da luz; a última camada é usada como câmada de atenuação, onde o padrão toma forma. Essas camadas são montadas e encaixadas no celular. Todas as camadas tem um furo no centro que é utilizado para a captura da imagem pelo celular. A configuração do dispositivo é apresentada na Figura A.2.

A partir do modelo descrito anteriormente foi implementado o nosso protótipo. A iluminação é forncedia por uma placa eletrônica com 36 LEDs, colocados em uma grade de 6 por 6. No centro desta placa foi feito um furo para a captura da imagem. A cima dessa, uma placa de acrílico com papel vegetal foi colocada para difundir a iluminação dos LEDs. Por fim, uma outra placa de acrílico foi colocada, também com papel vegetal, e uma transparência com circulos concêntricos impressos. Essa transpararência atenua a luz, fazendo com que os padrões sejam projetados. Estas duas camadas também tem furos

Figura A.3: Implementação do topografo proposto.

no centro. Na camada central também foi colocada uma lente para melhorar a capturada da imagem, como no modelo. A Figura A.3 mostra a implementação do protótipo.

Depois da captura da imagem dos padrões projetados vem a etapa do processamento destas imagens para que possamos estimar a superfície. Uma sequência de algoritmos é utilizada para: aumentar a qualidade capturada; extrair os padrões; e finalmente para a reconstrução da superfície.

Uma sequência de algoritmos de processamento de imagens é utilizada para melhorar a imagem e para a extração do padrão. A Figura A.4 mostra o estado inicial da imagem antes do processamento e o resultado depois desse processamento. Por fim, um algoritmo para reconstrução (DOSS et al., 1981; KLEIN, 1992) é utilizado para conseguirmos estimar a superfície.

A.2 Resultados

Nós analisamos os resultados conseguidos usando o método proposto de três maneiras. A partir das ceratoscopias conseguidas, a captura da imagem dos padrões após um processo de melhoria de qualidade; usando uma abordagem intuitiva utilizando os valores da decomposição da superfície reconstruída usando polinômios de Zernike (SCHWIEGERLING, 2004); e por fim, comparados os resultados obtidos com um equipamento comercial, o Pentacam (OCULUS, 2012).

Usando as ceratoscopias é possível ver as distorções geradas por diferentes condições. A Figura A.5 mostra exemplos de ceratoscopias conseguidas com o método proposto. Podemos observer diferenças nas formas dos padrões, que estão relacionadas a cada condição.

Analisando os valores dos coeficientes da decomposição da superfície reconstruída e os significados óticos de cada coeficiente, construímos uma tabela ordenada com os

Figura A.4: Processamento da imagem.

Ceratoscopias conseguidas para olhos com três condições. O olho normal tem padrões de forma circular A.6(a). Nos casos de astigmatismo os padrões se aproximam de elipses A.6(b). Por fim, os casos de ceratocones geram padrões ovais na imagem final A.6(c).

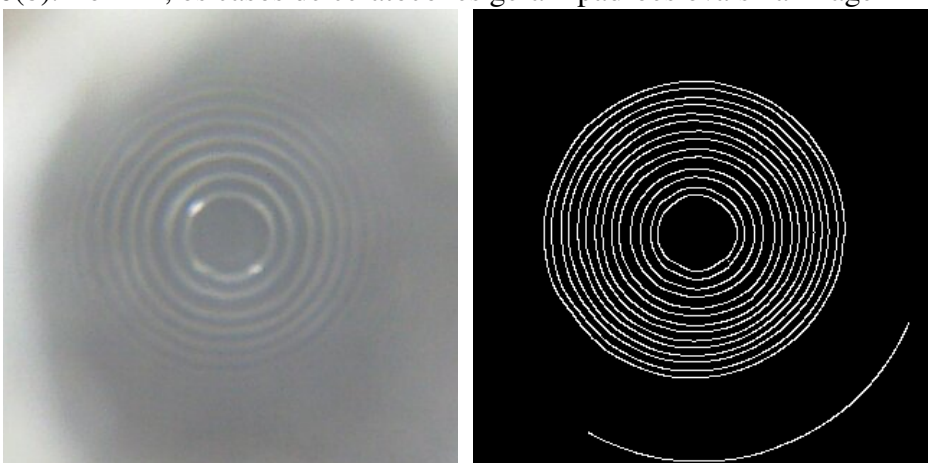

(a) Imagem inicial (b) Imagem após o processamento

Tabela A.1: Indivíduos com maior chance de ter ceratocone.

Usando o conhecimento dos polinômios de Zernike nós selecionamos os indivíduos com maior probabilidade de terem ceratocone. A tabela é ordenada pelos maiores coeficientes.

	Trefoil	Coma	Coma	Trefoil	Has keratoconus?
Subject 3	1.2282 μm	-1.188 μm	18.5596 μm	-5.6078 μm	yes
Subject 8	2.3114 μm	5.3911 μm	11.1504 μm	-2.994 μm	yes
Subject 4	-4.8245 μm	0.255 μm	5.6711 μm	-0.3516 μm	yes
Subject 6	-0.1445 μm	-1.3778 μm	2.7242 μm	-1.3965 μm	no
Subject 7	-0.5572 μm	0.5049 μm	3.2334 μm	0.3261 μm	no
Subject 9	0.2369 μm	-0.8915 μm	-2.9229 μm	0.3136 μm	no

sujeitos mais prováveis de possuírem ceratocone, a Tabela A.1 mostra os valores dos coeficientes com os sujeitos ordenados. Os três sujeitos classificados como mais prováveis nessa tabela, realmente possuem ceratocone.

Além disso, comparamos os valores da superfície gerada pelo Pentacam e o nosso protótipo. A Tabela A.2 mostra algumas estatísticas dessa comparação. Nós podemos ver que a diferença fica por volta de 0.02 milímetros aproximadamente. Para efeito de comparação, isso é o equivalente a 0.5% do raio médio da córnea (SCHWIEGERLING, 2004).

A.3 Conclusão

Este trabalho introduz um topografo de baixo custo e alta mobilidade, que nós chamamos de um topografo acessível. Olhando para os fundamentos dos discos de Plácido a intuição diz que é possível construir um dispositivo portátil e acessível. Nesse trabalho confirmamos essa intuição construindo este topografo.

Usando os princípios dos discos de Plácido, nós construímos um protótipo que junto com um celular captura imagens para o procedimento. Depois dessa captura, nós usa-

Figura A.5: Imagens das ceratoscopias.

Ceratoscopias conseguidas para olhos com três condições. O olho normal tem padrões de forma circular A.6(a). Nos casos de astigmatismo os padrões se aproximam de elipses A.6(b). Por fim, os casos de ceratocones geram padrões ovais na imagem final A.6(c).

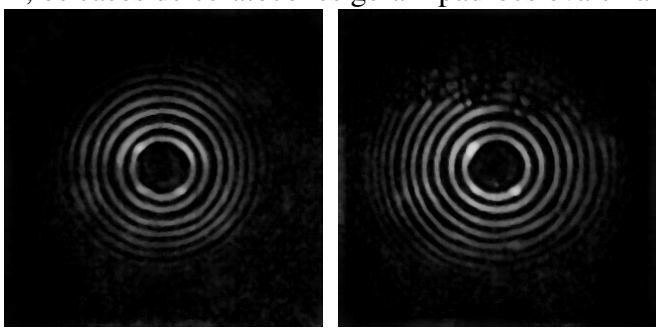

(a) Olho normal (b) Olho com astigmatismo

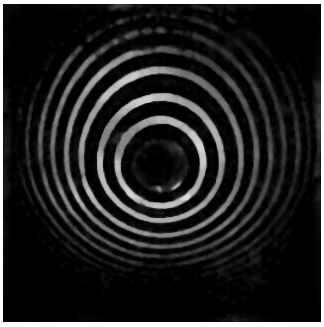

(c) Olho com ceratocone

mos uma sequência de algoritmos para melhorar a imagem e posterior reconstrução da superfície da córnea.

Nós avaliamos os resultados produzidos por esse trabalho de três maneiras. Primeiro, avaliamos as imagens capturadas e processadas, que chamamos ceratoscopias, e mostramos que é possível verificar algumas condições do olho utilizando essas imagens. Depois, usando a decomposição da superfície em valores com significado ótico, ordenamos os olhos com maior probabilidade de ceratocone, e os três classificados com maior chance realmente apresentam ceratocone. Finalmente, comparamos os nossos valores com um equipamento comercial onde a diferença média ficou por volta de 0.02 milímetros, o que para efeito de comparação equivale a 0.05% do raio médio da córnea humana.

Tabela A.2: Média e desvio padrão das diferenças das superfícies.

	Mean	Standard deviation
Eye 1	0.0401 mm	0.0225 mm
Eye 2	0.0350 mm	0.0202 mm
Eye 3	0.0211 mm	0.0218 mm
Eye 4	0.0280 mm	0.0296 mm
Eye 5	0.0224 mm	0.0144 mm
Eye 6	0.0254 mm	0.0134 mm
Eye 7	0.0202 mm	0.0209 mm
Eye 8	0.0186 mm	0.0089 mm

Diante do exposto, nós concluímos que um dispositivo para fazer medições da córnea a baixo custo é possível. Obviamente, o cuidado é muito importante e não devemos economizar recursos nesta área. Porém, nós devemos desenvolver alternativas para aqueles que não tem acesso a tecnologia de ponta. Além disso, dispositivos acessíveis podem ser usados em pré-triagens, onde pessoas com indicação de algum problema podem ser encaminhadas para atendimento mais específico.